Effect of heavy ion irradiation dose rate and temperature on α' precipitation in high purity Fe-18%Cr alloy

Yajie Zhao, Arunodaya Bhattacharya, Cristelle Pareige, Caleb Massey, Pengcheng Zhu, Jonathan Poplawsky, Jean Henry, Steven Zinkle

https://doi.org/10.1016/j.actamat.2022.117888
Acta Materialia 231 (2022) 117888

Effect of heavy ion irradiation dose rate and temperature on α' precipitation in high purity Fe-18%Cr alloy

Yajie Zhao [a,*], Arunodaya Bhattacharya [b], Cristelle Pareige [c], Caleb Massey [b], Pengcheng Zhu [a], Jonathan D. Poplawsky [e], Jean Henry [d], Steven J. Zinkle [a,b]

[a] *University of Tennessee, Knoxville, TN 37996, USA*
[b] *Materials Science and Technology Division, Oak Ridge National Laboratory, Oak Ridge, TN 37831 USA* [c] *Groupe de Physique des Matériaux, UMR 6634 CNRS, Université de Rouen Normandie et INSA de Rouen Normandie, Avenue de l'université, 76801 St Etienne du Rouvray, France* [d] *CEA, DEN, Service de Recherches Métallurgiques Appliquées, Laboratoire d'Analyse Microstructurale des Matériaux, Université Paris-Saclay F-91191 Gif-sur-Yvette, France*
[e] *Center for Nanophase Materials Science (CNMS), Oak Ridge National Laboratory, Oak Ridge, TN 37831 USA*

Abstract

Cr-rich alpha prime precipitates (CrRP) induce hardening and embrittlement of FeCr alloys, but the ki- netics of CrRP formation due to particle irradiation are not well understood. In this study, Fe18wt.%Cr alloy in solid solution state and pre-aged to produce relatively coarse CrRP was irradiated with 8 MeV Fe ions. The irradiation conditions involved two midrange doses of 0.37 and 3.7 displacements per atom (dpa), a wide range of dose rates (10^{-5}–10^{-3} dpa/s) and temperatures (300–450 °C). The distributions of CrRP after irradiation were studied with atom probe tomography (APT). The critical irradiation conditions to suppress CrRP formation were identified as 300 °C and 10^{-3} dpa/s; CrRP formation occurred readily at lower dose rates or higher temperatures. From 0.37 to 3.7 dpa, CrRP were observed to slightly grow at 350 °C and strongly coarsen at 450 °C. Specimens with pre-existing CrRP evolved into a similar pre- cipitate distribution as detected after ion irradiation on solution annealed specimens at 300–350 °C to 0.37 dpa, indicating that the precipitate microstructure approaches a quasi-equilibrium for doses < 1 dpa. Limited shrinking of pre-existing CrRP was observed after irradiation at 450 °C to 0.37 dpa, indicating a higher recovery rate at this temperature. The evolution of CrRP is quantitatively explained by employ- ing corrections to the historic Nelson-Hudson-Mazey precipitate stability model, and a radiation modified precipitation mechanism is proposed to account for the competition between radiation enhanced diffu- sion and ballistic dissolution which results in the modifications on both size and solute concentration of CrRP.

High Cr ferritic-martensitic (FM) steels are used for a va- riety of fossil energy and other demanding environments, and are promising structural material candidates for the fuel pin cladding and wrapper tubes in fast fission reactors and the blanket/first wall structures in fusion reactors due to their excellent thermo-mechanical properties and irradiation tolerance such as void swelling resistance [1] . However, these steels are known to suffer from the well-known '475 °C embrittlement' phenomenon after long time thermal aging at intermediate temperatures, which is due to the formation of Cr-rich alpha prime precipitates (CrRP) [2] that result in the increase of yield stress and ultimate tensile stress, and decrease in the impact strength [3–5] .

The phase separation kinetics to form CrRP in Fe-Cr alloys is very slow under thermal aging conditions below ~400 °C due to slow diffusion of Cr in Fe matrix. For example, CrRP were not ob- served after aging for 2150 h at the relatively low temperature of 290 °C [6] , while well-formed clusters were observed at 500 °C [7 , 8]. The CrRP were observed to slowly evolve at 350 °C for an- nealing times up to ~20 years [9] . Under irradiation conditions, the kinetics of CrRP formation are largely accelerated by radiation enhanced diffusion, resulting in their formation after neutron ir- radiation in different test reactors over a wide range of tempera- tures [10–22] . Electron irradiations were also found to be effective in promoting this phase separation process as CrRP were observed after irradiation by electrons to relatively low doses (< 0.7 dpa) at temperatures as low as 300 °C [23 , 24].

The results regarding the behavior of CrRP after ion irradiation are limited and more complicated to understand. Historically, CrRP formation was usually never reported after ion irradiations. Only recently, their presence after ion irradiations has been revealed by some studies for irradiation temperatures around 300 °C [25–29] . The discrepancy regarding the presence versus absence of CrRP can be roughly correlated with the differences in dose rate, injected interstitials, cascade size and bulk Cr content. Harrison et al. re- ported the formation of CrRP in Fe-14Cr after irradiation by He ions at 10^{-3} dpa/s, at which the displacement cascade size was very small [27] . In other experiments which involved heavy ion ir- radiations to produce large damage cascades, CrRP were observed after

irradiation at dose rates ≤3 × 10^{-4} dpa/s in Fe-18Cr [28], and at dose rates ≤10^{-4} dpa/s in Fe-14Cr [25–27]. Until now, no CrRP were detected in FeCr alloys with Cr content ≤12% after heavy ion irradiations [30]. The results obtained after ion irradiation at temperatures above 300 °C are scarcely reported. Jiao et al. revealed CrRP in commercial alloys with ~12% Cr after irradiation with protons at 10^{-5} dpa/s and 400 °C up to 10 dpa [2]. Although the bulk Cr concentrations for these ion irradiation studies are different, they are all located in the two-phase region [31]. The conflicting results about the presence/absence of CrRP are attributable to a competition between radiation enhanced diffusion (which promotes the formation of CrRP) and radiation mixing/ballistic dissolution processes associated with energetic displacement cascades (which destroys nanoscale clusters and thereby suppresses CrRP formation) [28, 29, 32]. The self-diffusion of solute atoms can be accelerated by orders of magnitude during irradiation due to the supersaturation of point defects, which is controlled by both dose rate and temperature [33]. On the other hand, irradiation with heavy ions is capable of destroying precipitates by ion mixing, and this dissolution rate is determined by the dose rate. The ion mixing occurs in recoil implantation, cascade mixing and thermal spike phases of the damage cascade, of which the thermal spike mixing is known to be most effective for energetic displacement cascades [34, 35]. The stability of particles under irradiation ultimately depends on the balance between these two mechanisms (i.e. radiation enhanced diffusion and ballistic dissolution). In supersaturated alloys, CrRP become less likely to form at lower temperatures and higher dose rates, while they are more likely to be stabilized and/or coarsen at higher temperatures or lower dose rates. Models have been proposed by several researchers to simulate this behavior [32, 36-38].

One point to note is that not all observed CrRP in irradiated Fe-Cr alloys are fully developed to achieve the Cr content predicted by the thermal equilibrium phase diagram [31, 39, 40]. Except for the 97.5 at.% obtained from the small angle neutron scattering (SANS) method, in which this value was adjusted from Calphad calculation instead of directly measured [13, 41], Cr content closest to the equilibrium composition of 96 at.% was measured only after electron irradiation at 300 °C or neutron irradiation at 455 °C, followed by about 85 at.% measured after neutron irradiation at 300 °C [10, 11, 24]. Conversely, precipitates with Cr content between ~50–60 at.% were typically reported after neutron or ion irradiations [12, 14, 28] and even lower cluster compositions below 50 at.% after ion irradiations were reported in Refs. [2, 26]. There is no universally agreed reason to explain the presence of these undersaturated CrRP. It was tentatively attributed to a variety of possible effects including a non-classical nucleation process [7, 11], APT artifacts due to the difference in evaporation field [14], radiation modified steady state effects [12], the irradiation dose being too low for full phase decomposition [10], cascade ballistic mixing effects [11, 28], and the effect of alloying elements [42].

The mechanism of CrRP evolution under electron and neutron irradiation conditions has typically been categorized as solely a radiation enhanced precipitation phenomenon, in which the effect of irradiation is only to accelerate the kinetics, not to modify it in any way [10-13, 15, 16, 24]. The reasons for ignoring the possible contribution of radiation induced solute segregation processes are that CrRP has been observed only in samples with supersaturated Cr concentration [10, 12]. However, consideration of only radiation enhanced diffusion fails to explain the disappearance of CrRP and the existence of undersaturated Cr clusters in some irradiated samples [2,

25]. These effects might be associated with bal- listic dissolution of the nanoscale CrRP by energetic displacement cascades.

Although CrRP formation has been extensively studied in pre- vious years, several unresolved issues remain such as the discrep- ancy regarding the formation or absence of CrRP under ion irradi- ation, the existence of clusters with Cr contents below the ther- mal equilibrium values, and quantitative uncertainties regarding the mechanism(s) controlling CrRP formation and dissolution under irradiation. In general, it is currently not possible to accurately predict the critical condition (the lower bound of temper- ature and upper bound of dose rate) for CrRP formation or dis- solution under ion irradiations. Wide variances exist in the bulk Cr content, impurity atom content, temperature, injected ion type and energy, knock-on atom spectrum, dose rate and dose among different studies, which makes it difficult to directly compare the results from different researchers. In this study, we performed a systematic study of heavy ion irradiation over multiple tempera- tures and dose rates on Fe-18 wt.%Cr (named Fe-18Cr in the sub- sequent text) samples. The high Cr content, which is well above the solvus line, was selected to provide a strong driving force for CrRP formation and high purity materials were utilized to mini- mize potential effects of impurity atom species such as C, N, O, etc. The irradiation conditions were carefully selected and controlled to study the effect of temperature, dose rate and dose. The objec- tive is to obtain the threshold irradiation condition for α/ α' phase separation and to study the kinetics for CrRP evolution under ion irradiations.

Table 1
Chemical composition of the as-received Fe-18Cr specimen. Note that a composition of 19.2 at.% Cr corresponds to 18.1 wt.% Cr in Fe. The statistical errors are the standard deviations from multiple measurements.

Specimen	Technique	element concentration					
		Cr (wt.%)	Cr (at.%)	C (wt.ppm)	S (wt.ppm)	O (wt.ppm)	N (wt.ppm)
Fe-18Cr	GDMS	17.97	19.05	7	2	6	5
	APT	18.08	19.2 ± 0.1	22 ±20	–	378 ±189	40 ±11

2. Experimental methods

2.1. Material

The Fe-18Cr alloy was manufactured by induction melting method in the European Fusion Development Agreement (EFDA) program. Cold reduction followed by heat treatment at 850 °C was performed to produce a recrystallized state with pure ferrite. The average grain size was 650 μm and dislocation density was less than 10^{12} /m^2 [8] . The nominal chemical composition, measured by Glow Discharge Mass Spectrometry (GDMS), and the chem- ical composition of the as-received sample we measured using APT are listed in Table 1 . APT measurement provided a Cr content of 19.2 ± 0.1 at.% (18.1 wt.%) (All the concentrations mentioned in the later sections are in at.% if not specified) with minor tip to tip variances, which is consistent with the reported nominal value. However, the APT-measured contents of impurity atoms are higher than the nominal ones, which might be partially attributed to tip preparations using focused ion beam (FIB) judging from the large statistical errors. Oxygen atoms were observed to be mainly located at the top surface of APT needles, which was very likely to come from the transferring from FIB to APT or long term stays in the chamber before running, while carbon and nitrogen were homogeneously distributed in the whole tip vol- umes. APT confirmed the lack of observable CrRP in the as-received samples.

Table 2
The midrange conditions for irradiations performed in this study. The symbol × indicates the conducted experiments.

Final dose (dpa)	0.37			3.7	
Temperature (°C)	300	350	450	350	450
10^{-3} dpa/s	×	×	×		
10^{-4} dpa/s	×	×	×	×	×
10^{-5} dpa/s			×		

A subset of the specimens were sealed in a glass tube with a vacuum environment (pressure of ~1–1.5 × 10^{-2} torr) and ther- mally aged to produce CrRP at 500 °C for

900 h followed by air cooling outside the furnace, with an initial cooling rate of ~10 to 20 °C/s. Due to the rapid cooling, and thus very short time at elevated temperatures, and the slow diffusivity of Cr at temper- atures < 400 °C, additional precipitation from Cr atoms in matrix during the cooling process is expected to be negligible. All the annealed and aged samples were subsequently mechanically pol- ished and finished with 0.05 μm colloidal silica. The final sam- ples were in disk shape with a diameter of 3 mm and thickness of 0.2–0.4 mm.

2.2. Ion irradiation experiments

Ion irradiations were performed with the 3 MeV Tandem parti- cle accelerator at the Michigan Ion Beam Laboratory (MIBL). Plasma cleaning of the sample surface for 2 h was conducted before irra- diation to reduce carbon contamination. The irradiations were per- formed between 300 and 450 °C for two ion fluences: 8.8×10^{14} and 8.8×10^{15} ions/cm^2. A defocused beam of 8 MeV Fe ions was used to create a total range of ~2 μm. The irradiation conditions are listed in Table 2 , which covers a wide range of dose rates and temperatures. The temperatures for the overall sample holder and each individual sample were measured using thermocouples and a 2D thermal imager to ensure no beam induced heating occurred. The variance of the individual specimen to target temperature was less than 6 °C. The target chamber pressure was maintained within 10^{-8} to 8×10^{-7} torr throughout the irradiations. The ion fluxes and irradiation times ranged between 2.5×10^{10} to 2.5×10^{12} ions × cm^{-2} s^{-1} (dose rates: 10^{-5} to 10^{-3} dpa/s) and 6 min to 9.7 h respectively.

Fig. 1 gives the depth-dependent distribution of irradiation dose and injected ion concentration predicted using SRIM-2013 for the 0.37 dpa midrange dose condition. The calculation was performed using the full-cascade mode and damage energy method with the displacement energy of Fe set to 40 eV [43] (the results are com- pared to the Kinchin-Pease Quick Calculation mode in Section 1 of the Supplementary). The analysis region was taken from the mid- range (depth ~1 μm) as denoted in the figure to minimize the po-

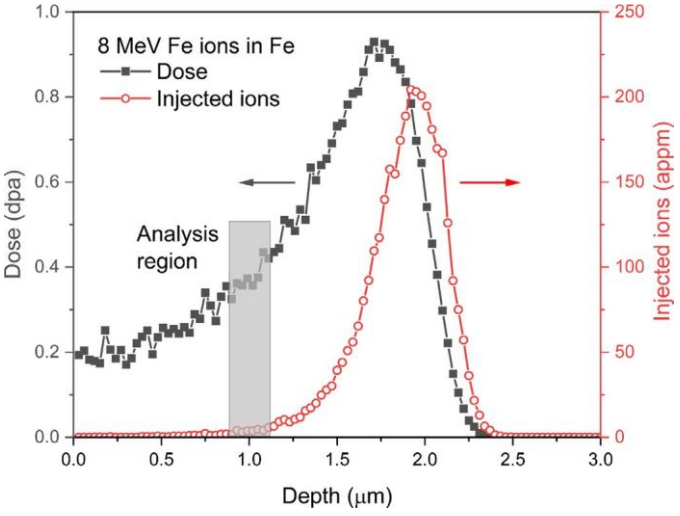

Fig. 1. SRIM prediction of the depth-dependent displacement damage and injected ion concentration of pure Fe irradiated by 8 MeV Fe ions to 8.83×10^{14} ions/cm^2, corresponding to the low fluence irradiation. Both values are 10 times higher for the high fluence irradiation. The analysis depth is marked by the gray-shadowed area.

tential anomalous contributions from both the surface and injected ions [44].

2.3. APT characterization

APT specimens were prepared through the FIB lift-out method. A length of around 800 nm below the platinum cap was removed by Ga beam sputtering in the final polishing step to access the desired mid-range irradiated region (irradiated depth of ~1 μm, Fig. 1). The APT runs were performed in voltage mode using a CAMECA LEAP-40 0 0X HR having a detection efficiency of 36%. The datasets were collected using a pulse rate of 200 kHz, a pulse frac- tion of 20%, and a detection rate of 0.3–0.5%. The

temperature in the analysis chamber was cooled down to 50 K to minimize the preferential evaporation of Cr atoms.

The reconstruction of the as-collected data was performed us- ing the Integrated Visualization and Analysis Software (IVAS) 3.8.4 developed by CAMECA, and the parameters used were the same for each dataset: 33 V/nm evaporation field and 1.65 compression factor. The field factor k was determined by fitting the interplanar spaces along the < 110 > or < 200 > directions. Despite all precau- tions including plasma cleaning [45] , carbon uptakes of 258–1474 appm during ion irradiations or FIB preparations were revealed by APT. Most carbon atoms were distributed homogeneously in the bulk. However, in several datasets, they were observed to segre- gate to dislocations or form C-enriched clusters of very low density (shown in Fig. S1 of the Supplementary). Cr segregating to poles was observed in all datasets (shown in Fig. S2 of the Supplemen- tary). All these microstructural features were removed before per- forming the analysis of CrRP.

The numerical results of Cr clustering were obtained through 3 methods: a statistical method modified from Ref. [46] to measure the Cr clustering in each dataset, a solute concentration-based clustering searching algorithm written with Python codes, and the isoconcentration interface or proximity histogram [47] .

The method in Ref. [46] measures the level of Cr clustering by comparing the standard error(s) of the experimental results with the standard deviation of the binomial distribution (σ). To quantify the difference compared to solid solution state, here we introduce a quantity named clustering coefficient as defined by Eq. (1) , in which N_b is the block size. A larger clustering coefficient indicates more clustering or phase separation in the dataset.

$$clustering\ coef\,icient = \sum_{N_b=50}^{500} (s-\sigma)^2 \quad (1)$$

The samples have been confirmed to be a random solid solution of Fe and Cr atoms before irradiation through this method.

The solute cluster search analysis was first conducted using the maximum separation method inherent to IVAS according to the D_{max} and N_{min} selection algorithm described in Ref. [10] , but misleading results inconsistent with the statistical results (clus- tering coefficient) were obtained (shown in Section 4 of the Supplementary). Therefore, we have developed a modified solute concentration-based filtering algorithm using Python to identify Cr-enriched clusters to calculate their radius, number density and volume fraction. This algorithm is similar to the one mentioned in Refs. [30 , 48], which was found to be more effective in identify- ing clusters in concentrated alloys than the maximum separation method [49] . Initially, by using the open-source software 3Depict [50] , the local Cr concentration at each atomic position was cal- culated. A threshold concentration of 30 at.% Cr was then applied to filter the atoms into potentially clustered atoms. The selected atoms form clusters if their separation distances were shorter than 0.5 nm and clusters with less than 16 atoms (N_{min}) were removed. The selection of these two parameters was based on the results of maximum separation analysis performed on the same datasets us- ing the method proposed in Refs. [10] . Background clusters were subtracted [51] . The envelope and erosion procedures were per- formed to remove the Fe shells outside of the clusters if there were any [52] . Heavily connected clusters were separated at the last step [7] . More details about this algorithm, the selection of parameters, and plots comparing results obtained from different methods are given in Section 5 and 8 of the Supplementary.

The solute cluster number density was calculated from the number of clusters divided by the tip volume and the volume frac- tion is the ratio of the number of atoms in clusters to the total number of atoms in the whole dataset. The solute cluster radius (R) was calculated from the number of atoms N_{prec} in each cluster with Eq. (2) , assuming the atomic density ρ= 84 . 3 $atoms/nm^3$ is identical to pure Fe [10] , and Q is the detection efficiency.

$$R = \sqrt[3]{\frac{3N_{prec}}{4\pi\rho Q}} \quad (2)$$

The Cr concentrations in matrix and clusters were obtained through the method of isoconcentration interface and proximity histogram (proxigram). Bachhav et al. proposed to use the concen- tration leading to

maximum number of interfaces as the threshold value [10] . Similar tests have been conducted on the datasets col- lected after irradiation to 0.37 dpa from as-received state, which provided threshold values of 21.5–27.5%, and most of them were smaller than 24%. However, using 21.5% resulted in high density of clusters after irradiation at 300 °C and 10 −3 dpa/s, and the matrix solute concentrations were incorrectly low. Since all the specimens have comparable bulk solute content, a constant threshold value for all datasets seems to be more reasonable. A threshold value that is too large can lead to the neglect of small and dilute clusters, and the splitting of large precipitates. However, if the thresh-

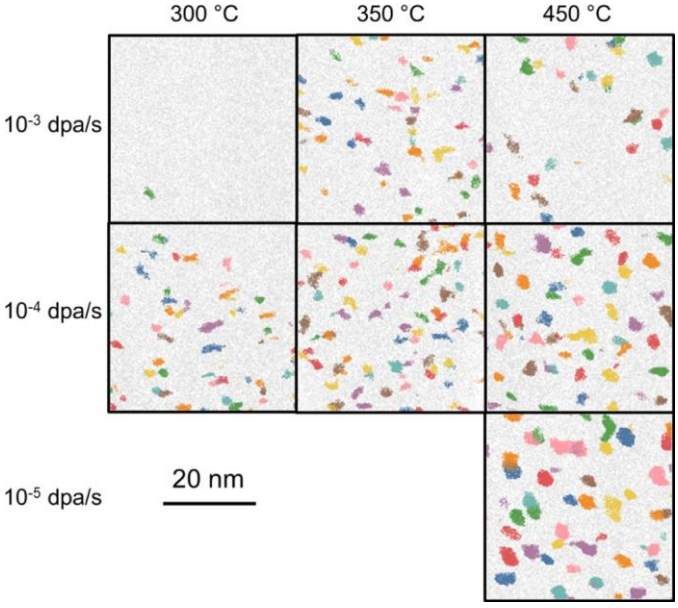

Fig. 2. Cluster atom maps showing CrRP in Fe-18Cr irradiated to 0.37 dpa. Sam- pled volume = 40 × 40 × 10 nm ^{3} . Clusters are indexed with different colors. All elements in the CrRP including both Fe and Cr atoms are shown.

old value is too low, cluster merging will happen and fake clusters will be generated, which leads to an underestimation of the ma- trix solute concentration. Therefore, an intermediate value of 24 at.% was selected for all the datasets. The core Cr concentration was obtained by fitting the proxigram with an empirical function [11] , and an example is given in Fig. S12 of the Supplementary. As the proxigram passes the interface and extends into the matrix, the measured solute concentration in each bin decreases and then in- creases due to crossing into the other neighboring clusters. There- fore, matrix Cr content was taken from lowest points in the prox- igram, and 5 bins were averaged to give the final value. The peak overlap of Fe and Cr atoms at 27 Da in the mass spectrum was corrected based on the natural abundance of each isotope for all the concentrations reported here. The number density could also be obtained with this method by taking the ratio of the interface number to the analyzed volume. This value is less accurate due to the possible artificial interconnection of multiple clusters.

3. Results

3.1. CrRP formation after irradiation to 0.37 dpa: effect of dose rate and temperature

The plot of the clustering coefficient (as defined in Eq. (1)) for Fe-18Cr irradiated to 0.37 dpa can be found in Fig. S9 of the Sup- plementary. Compared to the pristine sample, Cr clustering could be observed in most irradiation conditions except for 300 °C and 10 $^{-3}$ dpa/s. An increase of the clustering level at higher tempera- ture or lower dose rate was revealed.

Fig. 2 shows the distribution of cluster atoms filtered by the Python cluster analysis program for the samples irradiated to 0.37 dpa. A large number of CrRP were revealed for most irradiation conditions. They were homogeneously distributed without clear association with point defect sinks such as dislocations and grain boundaries. At 300 °C and 10 $^{-3}$ dpa/s, only 1 cluster was found in the presented volume. It should be noted that this cluster is likely to originate from field effect artifacts due to the spatial relation to low index crystallographic poles

(shown in Fig. S3 of the Supplementary). Therefore, the critical irradiation conditions for the

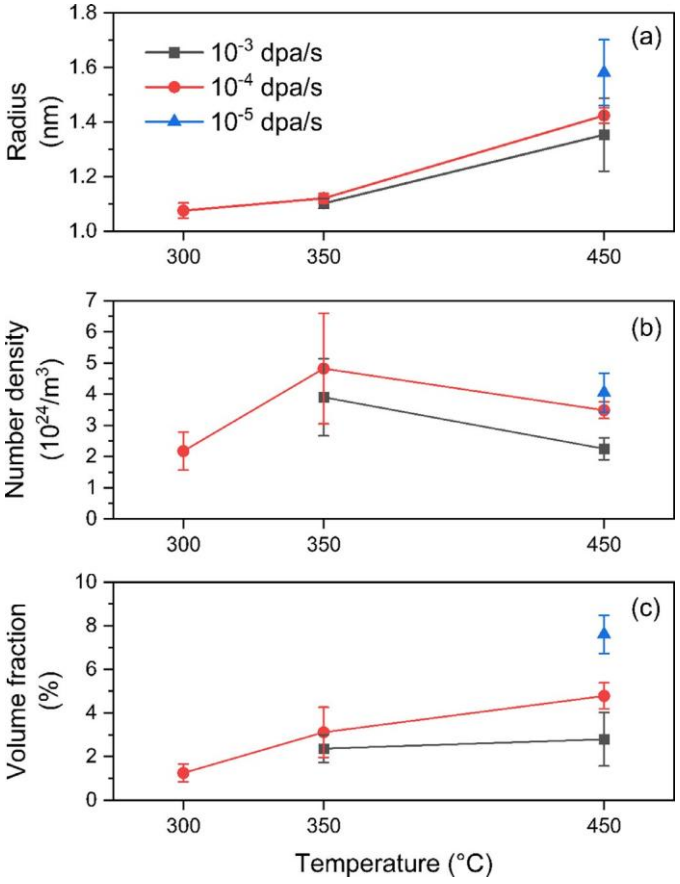

Fig. 3. The evolution of (a) radius, (b) number density and (c) volume fraction of CrRP in Fe-18Cr irradiated to 0.37 dpa at different temperatures and dose rates.

CrRP to dissolve or fail to nucleate as stable clusters are revealed as 300 °C and 10^{-3} dpa/s. For all other irradiation conditions, the APT artifact features would have a small influence on the cluster quantifications due to a large amount of observed cluster forma- tion and thus less Cr atoms being available for nonhomogeneous pole-line segregation artifact.

The evolution of radius, number density and volume fraction of CrRP with irradiation conditions are plotted in Fig. 3 . The average cluster radii were ~1–2 nm in all cases, which is consistent with the irradiated results in literature [10 , 12 , 14 , 24 , 26–28 , 30]. Cluster sizes increased with increasing temperature or decreasing dose rate. Within the range of investigated parameters, increasing the temperature from 300 to 450 °C had a much larger effect on clus- ter size than decreasing the dose rate from 10^{-3} to 10^{-5} dpa/s. The cluster number density was maximized at 350 °C for both investi- gated dose rates. This trend qualitatively agreed with the number density of isoconcentration interfaces obtained using IVAS (given in Fig. S11 of the Supplementary), although the latter method in- correctly provided smaller number density values for most condi- tions due to the presence of interconnected clusters which cannot be separated in the IVAS algorithm. The peak in CrRP density at 350 °C is likely due to the competition between coarsening (dom- inant at 450 °C) and dissolution by damage cascades (dominant at 300 °C). Increasing the dose rate decreased the number density at all temperatures, and it was most significant at 300 °C, at which the high dose rate 10^{-3} dpa/s led to disappearance of CrRP (or below the practical number density detection limit of ~10^{21} /m^3 within APT datasets containing ~35 million ions in our experi- mental examination). The highest volume fraction of CrRP (~7.6%) occurred after irradiation at 450 °C and 10^{-5} dpa/s (correspond- ing to ~10 h irradiation time), with a value close to the saturated volume fraction (~6.9%) for the same Fe-18Cr thermally aged at 500 °C for 2008 h [8] . The trend of volume fraction change, com- bined with the radius and number density evolution, agreed with nucleation, growth and Ostwald ripening of precipitates, the kinet- ics of which decreased with lower temperatures or higher dose rates.

The Cr concentration in the precipitates and matrix was cal- culated from the APT proxigrams. The matrix Cr concentration is presented in Fig. 4 (a). The bulk Cr content was obtained from the whole sampled volume averaged over all collected datasets. The matrix Cr content was ~14 at.% after irradiation at 450 °C and 10^{-5} dpa/s. This was close to the concentration obtained from the same alloy after thermally aging at 500 °C for 2008 h [8] . For all other irradiation conditions, the matrix Cr contents were much higher than the 9–14 at.% predicted by the phase diagram and other stud- ies in the temperature range of 30 0–50 0 °C [7 , 10 , 31]. At all tem- peratures, the matrix Cr concentration was lower at lower dose

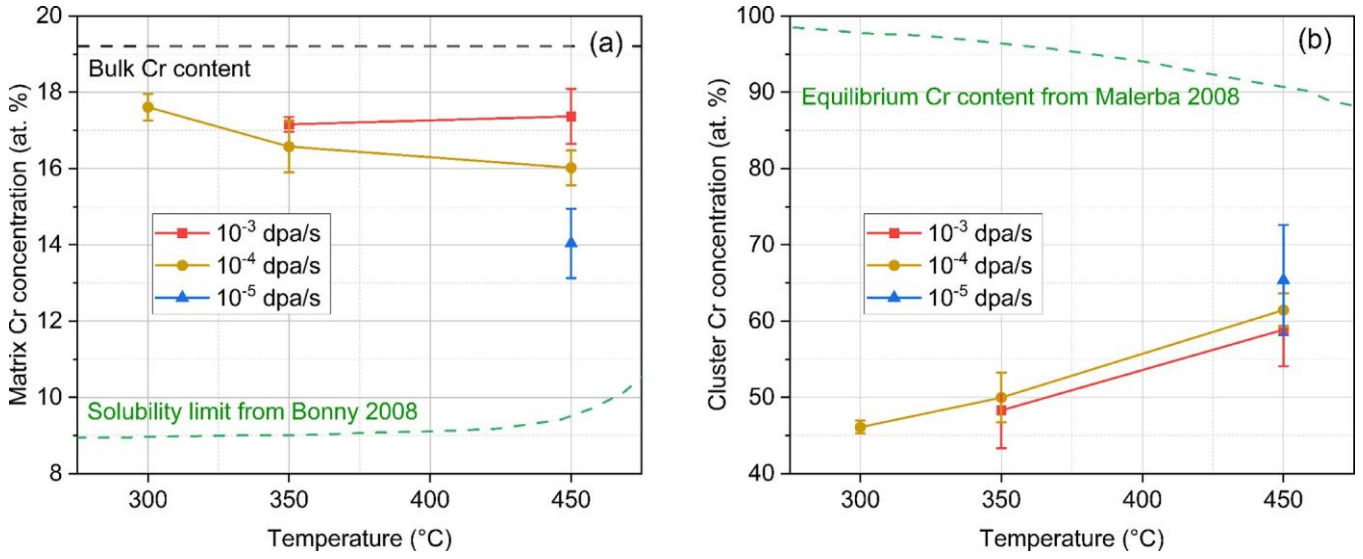

Fig. 4. The evolution of Cr concentration in (a) matrix and (b) cluster core for Fe-18Cr irradiated to 0.37 dpa at different temperatures and dose rates. The solubility limit in (a) and the equilibrium Cr content in (b) are reproduced from [31] and [53] respectively.

Table 3

The characteristics of CrRP in Fe-18Cr irradiated at 10^{-4} dpa/s, 350 and 450 °C, to 0.37 and 3.7 dpa. Data for the sample aged at 500 °C for 900 h, as obtained from APT data analysis, is also presented.

Aging temperature	Irradiation			Radius	Number density	Cluster core Cr	Matrix Cr content	
				1.12 ± 0.02	4.8 ± 1.8	50.0 ± 3.2	16.6 ± 0.7	3.1 ± 1.1
				1.29 ± 0.01	4.0 ± 0.7	57.9 ± 7.3	15.4 ± 0.5	4.1 ± 0.8
				1.42 ± 0.03	3.5 ± 0.3	61.5 ± 2.2	16.0 ± 0.5	4.8 ± 0.6
				2.01 ± 0.08	0.94 ± 0.06	66.3 ± 3.5	16.3 ± 0.3	4.2 ± 0.2
(°C)	temperature (°C)		Dose (dpa)	(nm)	(10^{24} /m^3)	content (at.%)	(at.%)	Volume fraction (%)
–	350	0.37						
–	350	3.7						
–	450	0.37						
–	450	3.7						
500/900 h	–		–	2.85 ± 0.34	0.51 ± 0.21	83.2 ± 5.3	14.4 ± 0.3	6.2 ± 0.6

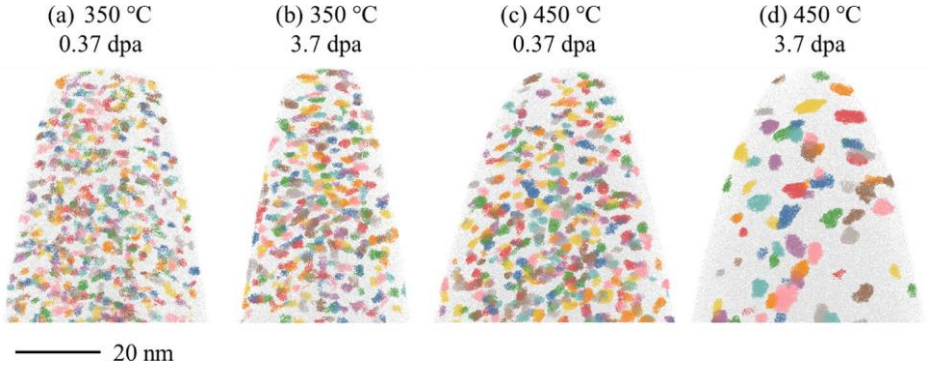

Fig. 5. APT reconstructions of Fe-18Cr samples irradiated at 10^{-4} dpa/s showing CrRP. The irradiation temperature and final doses are overlaid. All elements in CrRP including both Fe and Cr atoms are shown.

The Cr concentrations at the core of clusters are plotted in Fig. 4 (b). They were relatively widely distributed, ranging from ~45 to 65 at.% depending on the irradiation conditions. The core concentrations increased monotonically with increasing irradiation temperature. The ~10% increase in cluster Cr concentrations with increasing temperature from 350 to 450 °C compared to the neg- ligible or slight decrease in matrix Cr concentrations at both 10^{-4} and 10^{-3} dpa/s might at first seem contradictory. However, if the precipitate volume fraction (< 5%) is considered, the change in clus- ter Cr concentration corresponds to the transfer of < 0.5% Cr atoms from matrix to precipitates, which is comparable to typical mea- surement uncertainties (Table 3). Besides, since only the core so- lute concentrations of large precipitates were measured through the proxigram method, the change in the core solute content of smaller precipitates and the average solute content in all precipi- tates might be smaller and couldn't be captured by this method. While the Cr enrichment levels in the solute clusters following ion irradiation (~45–65%) were indicative of progression toward fully formed CrRP, the measured Cr contents were significantly less compared to the 80–90% equilibrium Cr content expected for CrRP as determined from thermal aging experiments [7 , 8] or predicted by phase diagram [40 , 53]. However, the Cr contents in the clusters after ion irradiation at 300–350 °C were similar to ~35–50 at.% Cr reported previously after irradiation by self-ions at 300 °C to ~1 dpa for a dose rate of 3–6.1 × 10^{-5} dpa/s [26] . Although the equilibrium Cr concentration for CrRP decreases slightly with increasing temperature, the measured Cr content in clusters exhibited an opposite trend.

3.2. CrRP formation after irradiation to 3.7 dpa

Fig. 5 compares the representative APT reconstructions for Fe18Cr irradiated at 10^{-4} dpa/s for two different temperatures (350 and 450 °C) and two final doses (0.37 and 3.7 dpa). The proper- ties of these clusters are summarized in Table 3 . The number den- sity of CrRP showed a slight decrease (~20%) with increasing dose at 350 °C and a significant reduction (~4x) at 450 °C, which in- dicates the clusters grew only slightly between 0.37 and 3.7 dpa at 350 °C while a strong coarsening occurred at 450 °C over the same doses. This observation was supported by the cluster size (radius) distributions as shown in Fig. 6 . The cluster size distri- butions were single-peaked for both doses at 350 °C with only a slight shift to a larger size at the higher dose, which may indi- cate that the CrRP were still in the nucleation or metastable stage with little growth. However, the size distributions were very dif- ferent at 450 °C: there was only one sharp peak at 0.37 dpa, while a much wider size distribution existed for irradiations up to 3.7 dpa. This difference at two temperatures can be attributed to the much slower kinetics for phase separation at lower temperatures. The cluster Cr concentration increased only slightly after the dose increased by ten times at both temperatures. The change in ma- trix Cr content and the volume fraction of CrRP phase was mi- nor, which may indicate that saturation of the precipitation process with dose is largely complete already by 0.37 dpa. Since the evo- lution of precipitate sizes agreed with a classical Ostwald ripening mechanism, the radii measured at higher doses can be compared to the radii estimated using the LSW theory [54] . This theory pre- dicts negligible size change (no change at 350 °C and negligible increase at 450 °C) if the thermal equilibrium vacancy concentra- tion is used, so the larger increase in precipitate radius measured through experiments indicates the accelerated growth or coarsen- ing rate of CrRP by irradiation, due to the supersaturation of vacancy concentrations. However, a radius of ~11 nm at 350 °C and ~16 nm at 450 °C after irradiation to 3.7 dpa is anticipated if the calculated radiation enhanced diffusion rates are used, which are much larger than the precipitate size measured through APT characterization. This again indicates the presence of strong ballistic dissolution effects, that effectively retard the precipitate coarsening rate.

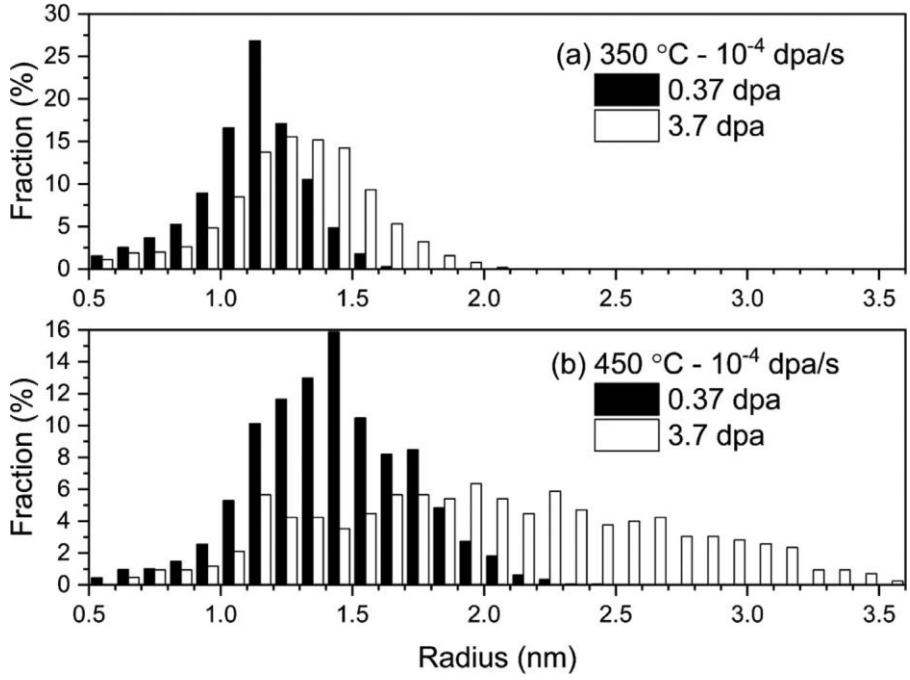

Fig. 6. Evolution of the CrRP radii distribution after irradiation at (a) 350 °C, 10 $^{-4}$ dpa/s, and (b) 450 °C, 10 $^{-4}$ dpa/s. Final doses were 0.37 and 3.7 dpa.

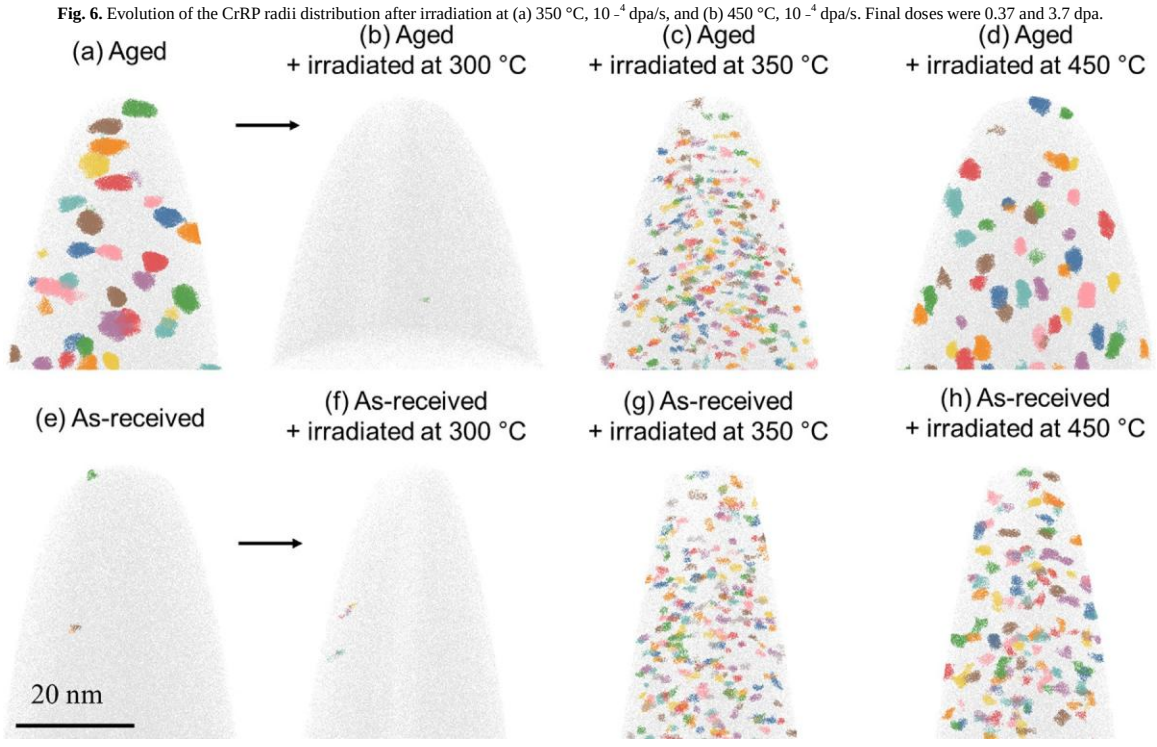

Fig. 7. APT reconstructions showing CrRP evolution in Fe-18Cr. (a) Sample aged at 500 °C for 900 h. Samples aged at 500 °C for 900 h followed by ion irradiation at (b) 300 °C, (c) 350 °C and (d) 450 °C. (e) Unirradiated as-received material. Samples that were ion irradiated from the as-received state at (f) 300 °C, (g) 350 °C and (h) 450 °C. The dose rates and doses were10 $^{-3}$ dpa/s and 0.37 dpa for all the irradiated specimens.

3.3. Ballistic dissolution of CrRP by irradiation in thermally aged Fe-18Cr

A portion of Fe-18Cr samples were thermally aged in a vacuum environment at 500 °C for 900 h to form CrRP. A representative APT reconstruction showing these precipitates is given in Fig. 7 (a). Well-formed CrRP were observed with an average radius of about 3 nm. The cluster core Cr content was measured to be 83.2 ± 5.3 at.%, which is very close to equilibrium values and in full agree- ment with the existing experimental values [7 , 8 , 53]. Only a few potential clusters were identified in the as-received sample by the Python codes due to the pole segregation artifact.

Both aged and as-received samples were then simultaneously irradiated at 300, 350 and 450 °C to 0.37 dpa (10^{-3} dpa/s). The reconstructions showing the evolution of CrRP precipitation are presented in Fig. 7 . At 300 °C, no formation of CrRP in the solid so-

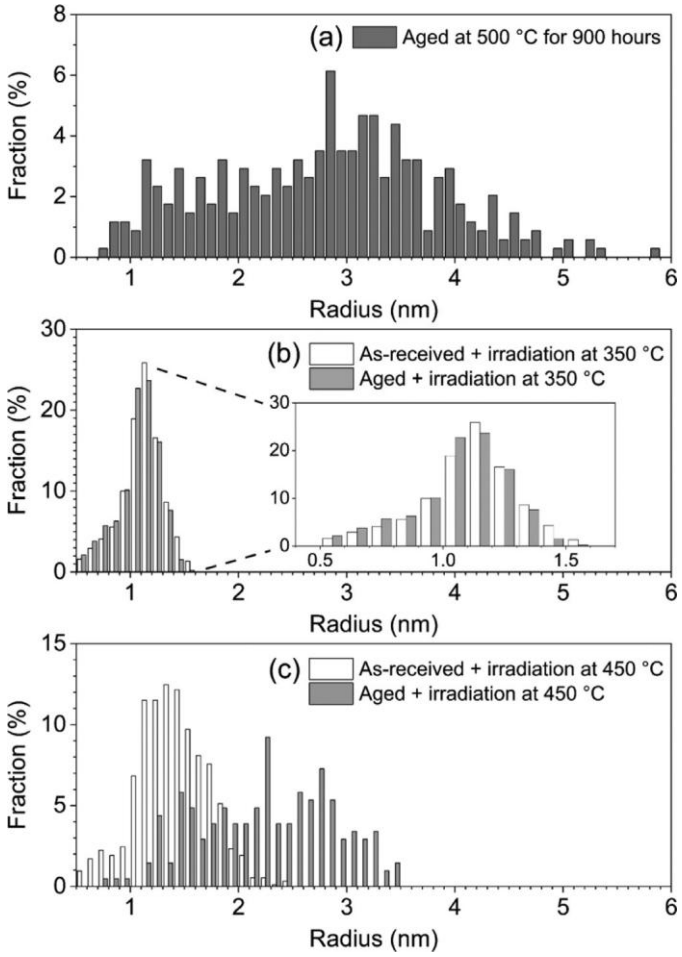

Fig. 8. Size distribution of CrRP (a) after aging at 500 °C for 900 h, (b) irradiation at 350 °C, 10^{-3} dpa/s to 0.37 dpa from aged and as-received state and (c) irradiation at 450 °C, 10^{-3} dpa/s to 0.37 dpa from aged and as-received state.

lution alloy and complete dissolution of CrRP in aged specimens were observed. At 350 °C, the large CrRP formed from thermal ag- ing were replaced by a high density of finer precipitates, and a similar microstructure was observed in the alloy irradiated from solid solution state. At 450 °C, differences in CrRP in the irradiated aged sample versus irradiated as-received sample were limited just based on the reconstructions.

Quantitative results including the radius distribution, average radius, number density, and volume fraction of CrRP, and the Cr concentration in the precipitate and matrix for the samples with precipitates are plotted in Figs. 8 and 9 . After irradiation at 350 °C, the clusters in the aged specimen shrank to a size distribution comparable to the sample irradiated directly from the as-received solid solution state (Fig. 8). The number density of clusters in the aged + irradiated sample similarly increased to a value comparable to the sample irradiated from the pristine state (Fig. 9). Further- more, the cluster volume fraction and Cr concentration in the ma- trix and cluster core following irradiation were very close for the two conditions (as-received vs. aged). These results indicate that the CrRP distribution already reaches a steady state after a dose of only ~0.37 dpa at 10^{-3} dpa/s and 350 °C, irrespective of the pre- irradiation precipitate microstructure.

However, the cluster distributions in the aged and as-received specimens were different after irradiation at 450 °C. The average radius of CrRP decreased by nearly ~0.6 nm due to the irradiation as compared to the as-aged state, but it was much larger than the clusters in the specimen irradiated from the as-received state.

The radii of clusters in this specimen were more widely distributed and extended to larger values compared to the sample irradiated from a pristine state. From Fig. 8 (c), there were no clusters with radius > 3.5 nm in the aged + irradiated specimen. The change in the number density of clusters was negligible, but the volume fraction was largely decreased due to their smaller sizes. It is interest- ing to observe that the core Cr concentration in the aged sample was not obviously changed by irradiation at 450 °C. Since

the clus- ters forming directly from the matrix had much lower Cr concen- trations, these highly concentrated precipitates were more likely to be the remnants of clusters formed during thermal aging, the sizes of which were decreased by irradiation while the core com- positions were unchanged. The matrix Cr concentration of the aged sample was largely increased by the irradiation, and it is closer to the value of samples irradiated from the pristine state (see Fig. 9 e). This observation is direct evidence of the ballistic dissolution effect driven by displacement cascades, which continuously ejects solute atoms back into the matrix. Because the core of large clusters was not significantly modified, additional solute atoms that entered the matrix are likely to originate from the dissolution of interface or small clusters.

4. Discussion

4.1. Comparison with previous experimental and simulation studies

Until recently, there was no definitive observation of CrRP pre- cipitation in Fe-Cr alloys with Cr concentrations up to 18% after ion irradiation from room temperature to 500 °C and dose rates of ~10^{-4}–10^{-3} dpa/s to final doses of 1–60 dpa [25 , 30 , 55-58]. This is due in part to difficulties with detecting CrRP by conven- tional electron microscopy techniques: similar lattice parameters of nanoscale coherent Cr-rich precipitates as Fe-rich matrix com- bined with precipitate sizes close to TEM resolution limits. The pronounced ballistic dissolution of precipitate nuclei by energetic displacement cascades as well as potential injected ion effects for heavy ion irradiations [26] could also suppress CrRP formation.

In our study, CrRP were detected after irradiation at 300 °C and 10^{-4} dpa/s, but not after irradiation at the same temperature and 10^{-3} dpa/s, which is qualitatively consistent with a previous work by Pareige et al. [29] . They didn't detect any CrRP in solution an- nealed Fe-12Cr alloys after irradiation at 300 °C and 2.2×10^{-4} dpa/s with Fe ions [30] . It indicated that despite the large differ- ence in bulk Cr content and spatial proximity of injected ions to the analyzed region in Ref. [29] compared to our study, the critical dose rate for the CrRP dissolution at 300 °C is 0.2–1 $\times 10^{-3}$ dpa/s in both studies.

We observed pronounced CrRP formation after ion irradiation at higher temperatures or lower dose rates, which qualitatively agrees with some recent ion irradiation results. A comparison for the var- ious properties of CrRP after ion and neutron irradiation is pre- sented in Fig. 10 . The radii of clusters are around 1–1.5 nm af- ter irradiation at ≤ 350 °C over a wide range of several orders of magnitude in dose rates, and all larger size clusters were ob- served at ≥ 450 °C, which indicates that the cluster size is more sensitive to temperature than dose rate. As for the dependence of number density on dose rate, the present study and that by Tissot et al. [26] observed a decrease in number density with increas- ing dose rate, while an increase of cluster density with increasing dose rate was observed in Ref. [28] , and there is no clear trend when multiple works are compared together. It could be partly at- tributed to the effect of low energy injected ions [26] , the simul- taneous change of both dose rates and doses [26 , 28], difference in characterization method [27] and APT data analysis method [10 , 28] that could result in a large difference in the measured precipitate number density. An extremely low number density ~3×10^{21} m^{-3}

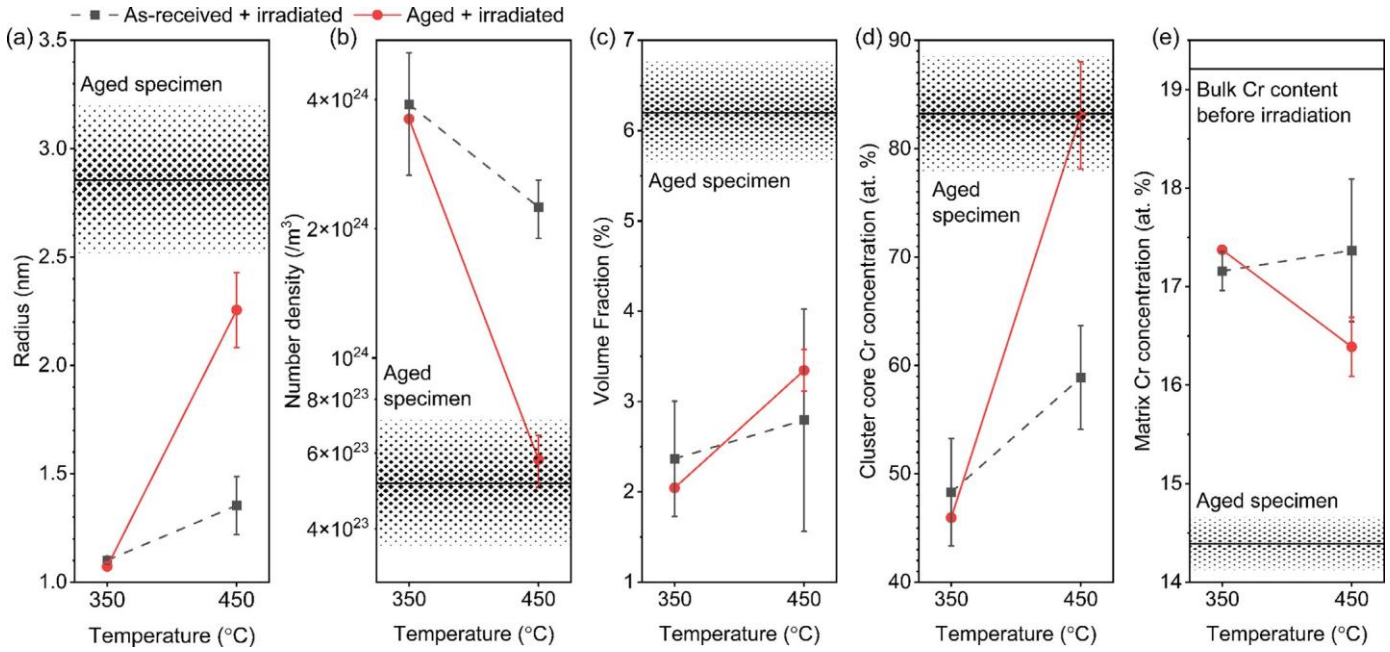

Fig. 9. Quantification of the CrRP. Comparison of the (a) mean cluster radius, (b) number density, (c) volume fraction, (d) Cr concentration in precipitates and (e) matrix Cr concentration. The investigated samples were Fe-18Cr irradiated at 350 and 450 °C, 10 $^{-3}$ dpa/s to 0.37 dpa and Fe-18Cr aged at 500 °C for 900 h followed with irradiations at same conditions. The shaded parts show parameters of CrRP formed from thermal aging. The horizontal lines represent the average values, and the half heights of the regions stand for the standard deviation of multiple measurements.

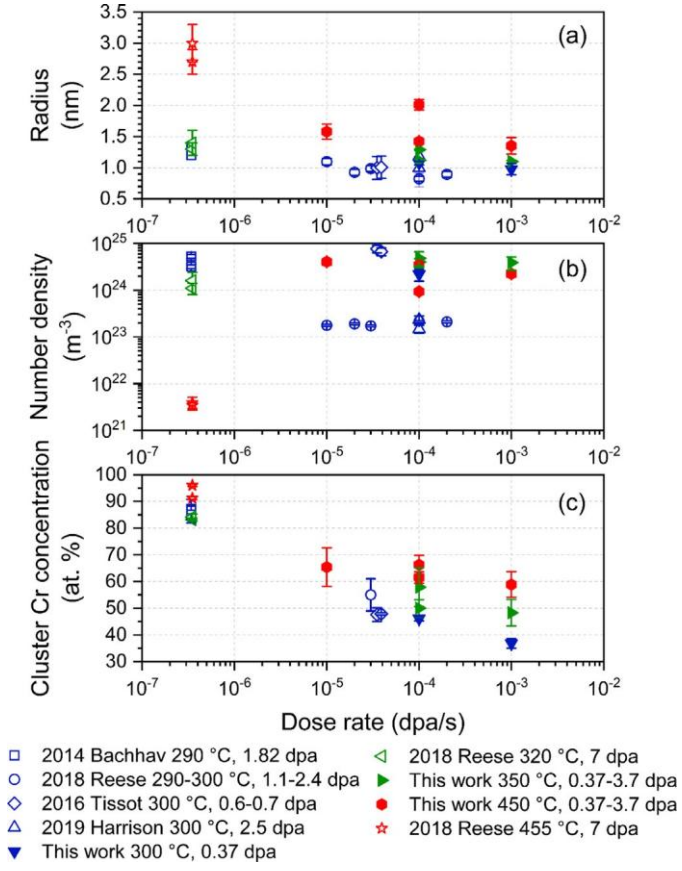

Fig. 10. Comparison of (a) radius, (b) number density and (c) Cr concentration of CrRP in Fe(15–19)Cr after ion (10 $^{-5}$ to 10 $^{-3}$ dpa/s) and neutron (~3 × 10 $^{-7}$ dpa/s) irradiation up to 7 dpa. The irradiations performed at temperatures ≥ 450 °C are presented with red symbols, 320–350 °C with green, and around 300 °C with blue symbols. Open symbols denote results from literature while solid symbols are from this work.

was measured by Reese et al. in Fe-(15–18)Cr after neutron irradia- tion at 455 °C, which seems problematic because a constant solute concentration in the alloy couldn't be maintained [11] . The clus- ter core Cr concentration monotonically decreased with increasing dose rate at all temperatures, with the highest Cr concentrations observed at the highest irradiation temperature for any given dose rate. The very high Cr concentration of ~80–90 at.% in the CrRP was achieved only after neutron irradiation at dose rates ~10 $^{-7}$ – 10 $^{-6}$ dpa/s. The Cr concentration is much lower for all the other high dose rate ion irradiation results, which will be discussed later in more detail.

Prior models of CrRP stability have conflicting predictions. An initial Atomistic Kinetic Monte Carlo (AKMC) simulation [59] sug- gested that accelerated diffusion by irradiation is the only signif- icant effect on the evolution of precipitates and that ballistic dis- solution effects are negligible at 290 °C. However, their more re- cent work used a combination of cluster dynamics and AKMC sim- ulations and found ballistic dissolution effects became important for ion irradiations with dose rates > 10 $^{-3}$ dpa/s [29] . The modeled precipitate dissolution was

mainly caused by the high sink densi- ties that reduced the point defect supersaturation, and thus it oc- curred at a relatively high dose of ~40 dpa at 300 °C. Although our experimentally determined critical dose rate of 10^{-3} dpa/s agrees with their predictions [29] , we observed complete dissolution of pre-existing CrRP already at 0.37 dpa, which is much lower than their estimation. Ke et al. used a phase field model to study CrRP formed after irradiation [60] . The authors concluded that irradia- tion dose rate controlled both radiation enhanced diffusion and ion mixing by causing replacements and displacements [60] . Our ex- perimental results clearly show decreased Cr clustering at a higher dose rate, which generally agrees with it [60] . But the critical dose rate of 10^{-5}–10^{-4} dpa/s predicted by Ref. [60] is much lower than our observations. This discrepancy might be partly attributed to the definition of CrRP between the simulations and our experimental results. A threshold Cr concentration of ~80% was selected to define the CrRP in [60] , which is much higher than the 30% we used for cluster analysis, and thus inevitably predicts a more conservative critical irradiation condition. Additionally, Ke et al. focused on Fe-15Cr, which has lower Cr supersaturation compared to Fe-18Cr used in this work and could potentially require a lower dose rate for the CrRP to be stabilized.

4.2. Mathematical modeling of the experimental results

Our work focuses on the formation of precipitates from solid solution or refinement of large precipitates to form finer ones. These precipitate stability cases were first evaluated in a simpli- fied model proposed by Nelson et al. (NHM model) in 1972 [32] . In their model, a precipitate can be dissolved by either recoil or disordering + diffusion mechanisms [32] . Since in Fe-Cr at tem- peratures below ~500 °C, the Cr-rich α and Fe-rich α phase form a continuous two-phase mixture between the end member pure Fe and Cr-based phases (without any intermetallic phases), irradiation induced disordering of either the precipitate or matrix is of sec- ondary importance. APT monitors the spatial distribution of differ- ent elements but does not detect atomic-scale order/disorder. Dis- ordering will not affect the APT detection of CrRP. Therefore, only the recoil dissolution mechanism is considered in this work, so the volumetric dissolution rate (dV/dt) of a precipitate with radius r is $\frac{dV}{dt} = -\frac{4\pi r^2 \phi}{N}$, where ϕ is the flux of recoils from the cluster to the matrix and N is the atomic density of the target. ϕ was ap- proximated as $\sim f_m G$, in which the multiplication factor $f_m \sim 10^{14}$ atoms/cm^2 ×dpa and G is the dose rate in dpa/s. The growth rate of a precipitate was listed as $\frac{dV}{dt} = 3D^{irr} cr/p$, in which the D^{irr} is the radiation enhanced diffusion coefficient, c and p are the atomic fraction of solute in the matrix and precipitates respectively. With the boundary condition of a constant total solute concentration C: $C = \frac{4}{3}\pi r^3 pn + c$, in which n is the number of precipitates per unit volume, the steady state precipitate radius could be calculated by setting equal to zero the derivative of the sum of the recoil disso- lution and regrowth coarsening terms:

$$\frac{dr}{dt} = -\phi + 3D_{irr}\frac{C - D_{irr}}{N r^2} = 0 \quad (3)$$

The radiation enhanced diffusion coefficient is $D^{irr} \approx f_v C_v D_v$ with f_v taken as the body centered cubic (BCC) correlation factor of 0.727 [61] . The vacancy concentration C_v can be calculated us- ing either recombination dominant or sink dominant approxima- tions [62] . The steady state vacancy concentration in the first case is $C_v \sim \frac{RG}{D_v D_i}$, in which $R = 4\pi r_c (D_i + D_v)$ is the point defect recom-

bination rate. The spontaneous recombination radius r_c is about 2.26a_0 with a_0 as the lattice parameter and as the atomic vol- ume [63] . $C_v = \sqrt{G}_{C_s}$ is the vacancy concentration for sink dominant conditions, in which $C_s = 4\pi rn$ is the sink strength of CrRP (as- sumed to be the dominant point defect sink). The diffusivity of a single vacancy (D_v) and interstitial (D_i) can be calculated using the migration energy for vacancies and interstitials in Fe-Cr as 0.67 and 0.34 eV respectively [64] .

Inserting the number densities measured from the APT results of this work and Tissot et al. [24] , and the equilibrium Cr content of α' precipitates, the original NHM model predicts that all the Cr atoms would be located in the precipitates, and the size of precip- itates is solely controlled by the number density (shown in Table S3 and S4 of the Supplementary). Possible reasons for this overesti- mation may include an underestimation of the ballistic dissolution rate or an overestimation of the precipitate growth rate. In addition, several of the terms used in the original NHM model appear to be incorrect.

We have made several science-based modifications to the original NHM model in an attempt to obtain more accurate estimates of the effect of particle irradiation on precipitate size. We note that the steady state vacancy concentration is overestimated if the dose rate is taken simply as the point defect production rate. To account for athermal in-cascade recombination of vacancies and interstitials and the additional correlated recombination that occurs at temperatures where point defects are mobile, the corresponding vacancy production efficiency should be around 0.1 to 0.2 [65– 67] . Additionally, the NHM model also overestimates the precipitate growth rate by including the entire matrix solute concentration. We have therefore modified the matrix solute concentration to be the solute supersaturation level by subtracting the solubility limit c_{eq} . One further modification is that the constant of 3 used in the original NHM equation for growth rate seems to be incorrect and should be replaced by 4 π [68] (the derivation is given in sec- tion 9 of the Supplementary). The equation for precipitate growth rate is therefore modified into:

$$\frac{dV}{dt} = 4\pi D_{irr}(c - c_{eq})r/p \quad (4)$$

As for the boundary condition of constant solute concentration, the original NHM equation is valid only for low volume fractions of precipitate. If the precipitate volume fraction might reach 5–10%, then the equation should be modified by the available matrix vol- ume fraction of $1 - \frac{4}{3}\pi r^3 n$, so the more precise boundary condition is:

$$p \times \frac{4}{3}\pi r^3 n + c \times \left(1 - \frac{4}{3}\pi r^3 n\right) = C \quad (5)$$

To test the effect of the modified growth rate on precipitate evolution, the experimental settings and number densities of CrRP reported after electron irradiations [24] were used, where bal- listic dissolution effects are negligible. The results are listed in the Supplementary file, section 9. Reasonable agreements on the steady state radii and doses to steady state for recombination- dominant conditions are achieved when the modifications summa- rized above are introduced. The sink dominant condition, on the other hand, results in an unreasonably high predicted dose (> 200 dpa) to achieve steady state due to lower radiation-enhanced dif-
fusion rates.

The recoil dissolution equation in the original NHM model used a multiplication factor of $f_m \sim 1/\sigma_d \sim 10^{14}$ for calculating the flux of recoils ϕ produced by a PKA, which is about an order of mag- nitude smaller than typical medium-mass ion displacement cross- sections of $\sigma_d \sim 10^{-15}$ cm^2 [69] . To get a more precise estimate of this recoil dissolution parameter, the mechanism through which the precipitate is dissolved by the displacement cascade is considered at the atomic level. During particle irradiations that in- volve damage cascades, most ion mixing occurs during the ther- mal spike phase, when a local high temperature region can form in the core of the cascade and replacements occur between neighbor- ing atoms [34 , 35 , 67]. The thermal spike phase has several impor- tant consequences: the recombination of a large portion of point defects, which is roughly quantified by the point defect produc- tion efficiency term, the direct formation of large defect clusters, which needs more complicated models to address and is out of the scope of this work, and atomic mixing, which enhances pre- cipitate dissolution and can be quantified by the replacement per atomic displacement

(RPA) parameter [67 , 70]. Considering a dis- placement energy of 40 eV and the injected ions energy of 8 MeV, the average energy of the primary knock on atoms is calculated to be ~15 keV, which is above the energy for sub-cascade formation. Thus, the number of replacements is linear with the damage energy, i.e. it can be correlated with the dpa value through a simple ratio [67 , 71]. Using SRIM-2013 simulations and a replacement per displacement ratio of $\xi_{rpa} \sim 50$ [60 , 67 , 72], the ballistic dissolution factor in the observed midrange depth region of this study is $f_m = 1.17 \times 10^{17}$ atoms/cm^2 ×dpa. However, the distances that most atoms travel during the thermal spike phase are short-

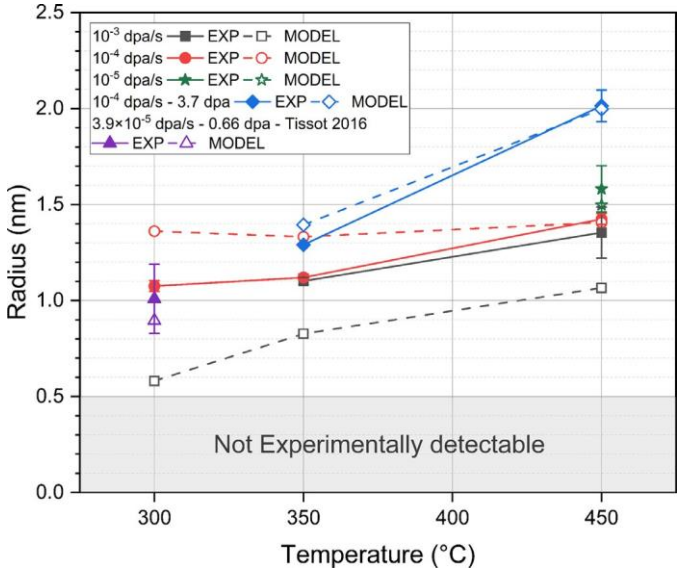

Fig. 11. Comparison between radii measured with APT (filled symbols) and calcu- lated with the modified NHM model (open symbols). The legends with EXP denote experimentally measured values from the current study and Tissot et al. [26] . The legends with MODEL denote calculated values from the modified NHM model.

ranged due to intense in-cascade recombination and the short time of only a few picoseconds. In an alternative derivation, the long- range displaced atoms are considered to be more important to the dissolution of precipitates as this can lead to direct ejection of solute atoms from the precipitates and direct injection of matrix solvent atoms into the precipitate. The corresponding ballistic dis- solution factor can be calculated with equations (14) and (16) in Ref. [73] and appropriate values reported in Ref. [74 , 75]. The result is $f_m = 1.4 \times 10^{16}$ atoms/cm^2 ×dpa if the fourth nearest neighbor distance was used to define the long-range displaced atoms (The detailed derivations of these two values are presented in section 9 of Supplementary file). Although the estimated ballistic dissolution factor using the subset of long-range displaced atoms is around 10 times lower than the factor calculated using the RPA value, both methods presented here suggest a much higher dissolution rate parameter compared to the original NHM model ($f_m = 10^{14}$ atoms/cm^2 ×dpa).

With these modifications, the revised equation to calculate the precipitate radius at steady state is:

$$\frac{dr}{\times 3 - 4\pi n r^3 - rp} \times \left(\frac{f_m G D^{irr} C}{3 - 4\pi r^3 n} + C_{eq} \right) = 0 \qquad \frac{D^{irr}}{4\pi r^3 np\, dt} = -N + rp \tag{6}$$

We observed that $f_m = 1.17 \times 10^{17}$ atoms/cm^2 ×dpa slightly underestimates the steady state radii compared to experimen- tal measurements in this work and the ion irradiation result by Tissot et al. [26] . On the other hand, using $f_m = 1.4 \times 10^{16}$ atoms/cm^2 ×dpa, the steady state radii were overestimated in most ion irradiation conditions (shown in Supplementary). Generally good quantitative agreements were achieved by as- suming recombination-dominant conditions with $f_m = 8 \times 10^{16}$ atoms/cm^2 ×dpa. The CrRP radii predicted for this case are com- pared to the experimentally measured values in Fig. 11 . For the cluster analysis of APT datasets, the N_{min} was set to be 16 atoms, which corresponds to a cluster with a radius ~0.5 nm, so any clusters with sizes smaller than 0.5 nm are not detectable by the current APT analysis method. At the irradiation

condition of 300 °C and 10^{-3} dpa/s, the predicted steady state radii are 0.58 nm assuming the number density of precipitates to be 10^{23} or 10^{24} /m^3, which is approaching the APT detection limit and consistent with our experimental observations. The overestimation of steady state radii with $f_m = 1.4 \times 10^{16}$ atoms/cm^2 ×dpa implies that the ex- clusion of atoms displaced less than four nearest neighbor dis- tances may not be appropriate; atoms that are ballistically dis- placed shorter distances may also contribute to precipitate disso- lution.

If sink dominant conditions are assumed (considering the po- tentially very large sink strength of CrRP), the modified NHM model predicts complete dissolution of precipitates at all con- ditions due to the low steady state point defect concentrations caused by high sink strength, no matter which of the two f_m val- ues are selected. This disagreement with our experimental obser- vations may indicate that CrRP have a weak interaction with point defects, which is reasonable because the lattice mismatch between α-Fe and α'-Cr is very small. The point defects in the vicinity of precipitates may not experience any noticeable strain field, and if they hop into the α- α' interface they might be weakly bound and easily desorbed. Therefore, the CrRP sink strength might be much smaller than predicted from the incoherent precipitate sink strength equation. Since the sink strength from other features such as network dislocations and dislocation loops was relatively low for the investigated irradiation conditions, the recombination- dominant approximation is considered to be appropriate to obtain steady state vacancy concentrations in this alloy system. This eval- uation is also supported by the better fitting of electron irradiated Fe-Cr precipitate results with recombination dominant conditions
[24].

4.3. The effect of carbon, irradiation conditions and starting precipitate distribution

Carbon contents of 258–1474 appm after the ion irradiations were revealed using APT. Although some introduction of carbon atoms by FIB preparations is very likely based on the large differ- ence in measured chemical compositions using GDSM or APT tech- niques (Table 1), the concentrations of carbon after ion irradiation were considerably higher than that measured in the as-received specimens, which indicated the occurrence of moderate carbon contamination during irradiations. Carbon atoms were present in the sampled volumes in 3 forms: segregating to dislocation loops or lines, forming Cr-containing carbides, and homogeneously dis- tributed in matrix. Segregation of carbon on dislocation loops can potentially stabilize the enrichment of Cr at or close to the loop core, and thus decrease the Cr atoms available for precipitate for- mation [58] . Carbides also act as sinks to reduce the concentration of point defects. In all the collected APT datasets, carbides were
observed only after ion irradiation at 450 °C, 10^{-5} dpa/s to 0.37 dpa. The lack of carbides at other conditions might be due to the relatively small analyzed volume using APT. Employing other tech- niques would be useful to verify their existence or absence at other conditions. In datasets where carbides were detected, their radius was 2.5 nm and number density was 1.4×10^{22} /m^3, which gave a sink strength of 4.4×10^{14} /m^2 and could largely decrease the local vacancy concentration near the carbide/matrix interface. Due to the strong binding of carbon with vacancies (V), the existence of carbon in solid solution could lead to the formation of C-V com- plexes [76] , within which C_2V (2 carbon atoms and 1 vacancy) and C_4V_2 are the most stable forms [77 , 78]. The effect of C_2V can be ignored due to the lower dissolution temperature of ~240 °C [78] . However, the dissociation temperature of C_4V_2 was measured to be ~357–377 °C, and its fraction within all complexes increases with carbon content, which implies it may contribute to reducing vacancy concentrations at 300–350 °C [78 , 79]. In short, the presence of carbon in all 3 forms results in the decreased Cr concentration available for clustering or decreased free vacancies for diffusion, and therefore likely slows down the CrRP formation kinetics. Since the effect of impurity carbon atoms was not considered in the modified NHM model, calculating the steady state vacancy concentration using recombination dominant approximation may lead to an overestimation of radiation enhanced diffusion rates, and in- troduce uncertainty on the determination of f_m value. However, because the interaction between carbon

and vacancies are compli- cated, and the migration energy of vacancies obtained from simu- lation works considering carbon effects varied within 0.83–1.3 eV [29 , 80], it is currently difficult to include it in the modified NHM model.

The irradiation temperature affects the CrRP evolution in both thermodynamic and kinetic aspects: it determines the solubility of Cr at thermal equilibrium and affects the radiation enhanced dif- fusion rate. For the temperatures investigated in this study (300 to 450 °C), the solvus line is expected to be in the range of 9–14%Cr and increases with higher temperature [7 , 10 , 13], which means the driving force for precipitation at higher temperatures will decrease due to the lower solute supersaturation, and the nucleation rate will be reduced accordingly. On the other hand, the diffusion rate will either increase or remain nearly constant with increasing tem- perature for recombination- and sink-dominant conditions, respec- tively. Since the ballistic dissolution of precipitates is independent of temperature, the promoted Cr clustering at higher temperatures indicates that the effect of increased diffusion rate is larger than the reduced driving force in the temperatures investigated here.

Precipitate stability is controlled by the competition between radiation enhanced diffusion and ballistic dissolution processes, and these rates both increase with increasing dose rate. However, since precipitate nucleation is a complex process, it is not quantita- tively accurate to simply compare the ratio of these two rates. The general expectation is that the effect of radiation enhanced diffu- sion is more important at lower dose rates, while ballistic disso- lution is more important at higher dose rates, which is consistent with the evolution of steady state precipitate radius we observed in this work.

The dose level controls the degree of microstructure evolution from its unirradiated starting point and toward the ultimate irra- diation steady state condition. In our study, only minor difference in precipitate number density and sizes was observed after irradi- ation to the high dose at 350 °C, which implies the steady state under irradiation has been achieved or was very close already at the dose of 0.37 dpa. On the other hand, there was a large differ- ence in precipitate distribution between these two doses at 450 °C. The increase in radius, decrease in number density and negligible change in volume fraction of precipitates (Table 3) agree with the classical Ostwald ripening mechanism. The same Fe-18Cr alloy was aged at 475 °C up to 900 h, which produced CrRP with an aver- age radius of 1.9 nm [81] . This is similar to the size of precipitates formed after irradiation at 450 °C to the high dose. However, the much shorter time taken by irradiation (~10 h) compared to ther- mal aging suggests the coarsening kinetics was largely accelerated by irradiation, implying the contribution from thermal coarsening is likely negligible. This radiation enhanced coarsening behavior is consistent with other systems such as the evolution of oxide par- ticles in ferritic steels and γ^{prime} precipitates in NiAl alloys dur- ing ion irradiation at 500–650 °C [82 , 83], and it was attributed to the irradiation created point defects, the concentrations of which are much higher than their thermal equilibrium values. We note a current shortcoming of the modified NHM model is the lack of a radiation enhanced coarsening term, so it is only relevant for low to intermediate temperatures and doses. This improvement will be considered in our future works.

In our study, Fe-18Cr specimens in the supersaturated solid solution state or with pre-existing well-developed (relatively coarse) CrRP were irradiated side-by-side at the same conditions. At the two lower irradiation temperatures, both states evolved into a similar microstructure of complete disappearance of precipitates at 300 °C or filled with a large number density of

nanometer-scale precipitates at 350 °C, which indicates that the starting precipitate distribution has a negligible effect on the steady-state precipitate microstructure and the irradiation-controlled steady state was achieved quite rapidly at 0.37 dpa under these ion irradiation conditions. Conversely, at 450 °C differences persisted between the precipitate distributions for irradiated specimens that were initially in the supersaturated solid solution vs. thermal aged conditions. The precipitate sizes were larger and the number den- sities were lower in the pre-aged sample (Fig. 9). This observa- tion doesn't necessarily imply that the starting precipitate distri- bution has an effect on the steady state, but it is more likely that a higher dose is required to achieve the steady state at this higher temperature. Since the dissolution rate is independent of the ir- radiation temperature, the different behavior at 450 °C compared to the two lower temperatures must be attributed to the differ- ent radiation enhanced diffusion rates. At 450 °C, the solute atoms might quickly diffuse back once they are dissolved by the displace- ment cascade, which maintains a relatively high solute concentra- tion and large size of the precipitates. Since Cr atoms prefer to in- teract with themselves to form CrRP in alloys with high Cr concentration, and the dissociation of C_4V_2 complexes lead to the re- lease of additional vacancies in case if there is too much carbon in samples [78] , the precipitate restoration kinetics associated with diffusion of dissolved solute atoms is also higher at 450 °C. Con- sidering the typical size of a displacement cascade or the spatial extent of the thermal spike phase, which is ~5–10 nm in diam- eter, it is anticipated that precipitates with sizes larger than this are less likely to be destroyed because the damage cascades hap- pening completely inside the precipitates are ineffective in causing ion mixing. Therefore, the higher diffusion rate, and the resulting larger driving force for precipitate re-growth and less efficiency of damage cascades, lead to the larger resistance of CrRP to ballistic dissolution at this high temperature.

The experimental observation that the steady state radius of CrRP is controlled by irradiation dose rate and temperature irre- spective of the starting size is in agreement with the predictions of the modified NHM model (Eq. (6)). Several examples comparing the evolution of precipitate sizes with irradiation dose predicted by the modified NHM model and experimental datapoints from this work, and ion, neutron and electron irradiation results in literature [10 , 24 , 26] are presented in Fig. 12 . The APT dataset from the work of Bachhav et al. has been reanalyzed [10] . Since we considered all precipitate atoms for radius calculation, the resulting radius was larger than what was originally reported. Reasonable agreements on both dose and CrRP radius are achieved for the diverse con- ditions of electron irradiation, ion irradiation at 300 °C and 10^{-3} dpa/s from either solid solution or aged state, and ion irradiation at 450 °C and 10^{-3} dpa/s from solid solution state. At the two ion irradiations and neutron irradiation that involve lower dose rates (10^{-5}, 3.9×10^{-5} and 3.4×10^{-7} dpa/s respectively), although the steady state radii were correctly reproduced by the modified NHM model, much lower doses are predicted by the model to reach the steady state. This suggests that the net growth rate is somewhat overestimated in the model predictions, which might be related to the loss of point defects at sinks that are not considered in the analysis, or the lower nucleation rate that causes prolonged nucleation regimes at these conditions. As for the sample with preexisting CrRP ion irradiated at 450 °C and 10^{-3} dpa/s, both the radius and saturation dose appear to deviate significantly from the model predictions, which might be attributed to the higher recovery rate of precipitates and lower efficiency of the displacement cascades. Although the modified NHM model correctly predicts the formation of CrRP under irradiation conditions used in Ref. [27 , 28],

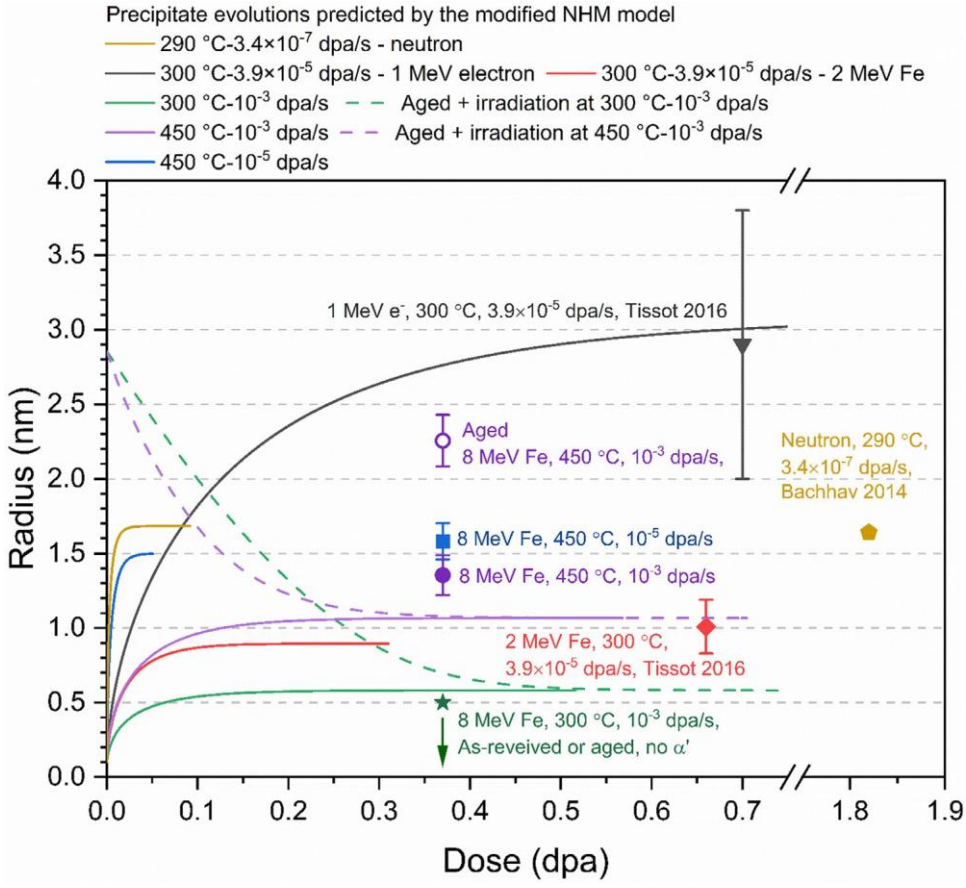

Fig. 12. Comparison between the evolution of CrRP radii with dose predicted with modified NHM model (curves) and the experimental measurements (isolated data points) for selected irradiation conditions [24 , 26]. The experimental datapoints are from irradiations performed on specimens in the solid solution state if not specified.

the steady state radii could not be well reproduced, which might originate from the difference in characterization and data analysis methods that can introduce large differences on the measured pre- cipitate number densities.

In general, good qualitative agreement on precipitate growth and shrinkage with experimental observations is achieved (in con- trast to large discrepancies with the original NHM model) due to the inclusion of more appropriate physical terms. The quantitative impacts of each modification on the steady state radii predicted by the modified NHM model are provided in section 9 of the Sup- plementary. The sizes of CrRP and the doses to reach saturation during irradiations were quantitatively accurately predicted for a large portion of irradiation conditions. The underestimation of re- quired dose for achieving steady state at conditions involving both low dose rates and displacement cascades might be related to un- certainties in the precipitate nucleation process and the number density change, which is important in both nucleation and coars- ening stages, and is not comprehensively included in this model. The better agreement with experimental observations by using re- combination dominant approximation indicates that CrRP may not be effective point defect recombination centers, despite their very high number density in Fe-18Cr after irradiation at 300–450 °C.

4.4. The mechanism of α' precipitation under ion irradiation conditions

In our study, all clusters formed after ion irradiations in asreceived specimens have Cr concentrations in the range of 40–75 at.%, which is much lower than the equilibrium Cr content in CrRP as presented in Fig 4 (b). This raises questions whether this might be an APT experimental artifact versus a true phenomenon [14] . The characterization of CrRP clusters with APT is known to suffer from the local magnification effect and ion flight trajectory aber- rations due to the lower evaporation field of Cr compared to Fe [84] . According to our analysis on the change of cluster core Cr content and atomic density as a function of their radii for thermal aged and ion irradiated samples (shown in the Supplementary Fig. S17), the smaller clusters have relatively lower solute concentrations, and their atomic densities (the increase of which is an in- dication of trajectory aberration) are not significantly higher than the theoretical value. On the other hand, the densities of larger precipitates are much higher and increase with their Cr contents, which implies the focusing of ion trajectories doesn't change the core solute concentration [85] , and the high solute concentration is responsible for the increase in local atomic density. This find- ing agrees with a previous simulation work, which found the ma- jor effect of local magnification is to modify the precipitate shape without changing the core Cr content [86] . Post-aging characteri- zation of CrRP using APT carried out by Novy et al. also excluded the possible contribution of trajectory aberration to decrease core Cr content by showing that similar sized-precipitates in specimens aged at different times exhibited different Cr concentrations [7] . Therefore, it appears the measured sub-equilibrium Cr content in the CrRP is mainly controlled by kinetic/thermodynamic aspects during irradiation.

A non-classical nucleation mechanism in which the CrRP nucle- ates with a solute concentration lower than the thermal equilibrium composition was previously proposed as an explanation for the appearance of low Cr content in the clusters formed from thermal aging or particle irradiation [7 , 11 , 87-89]. Although this mechanism might explain the formation of low Cr content for clusters in samples irradiated to low doses, it is not fully consistent with our observations. After irradiation at 450 °C and 10^{-4} dpa/s to 3.7 dpa, the Cr content of clusters was 66 at.%, although strong coarsen- ing has occurred, and close to equilibrium Cr concentrations were measured in precipitates of similar size after aging at 500 °C. Combining the results on ion irradiated samples with pre-existing CrRP, it appears that the cluster Cr content is affected by the irradi- ation conditions studied here instead of only by the equilibrium phase diagram and the non-classical nucleation process. This con- clusion is also supported by the measured matrix Cr content in the aged + irradiated samples, which is much higher than the solvus limit and can be attributed to the continuous ejection of Cr solute from precipitates into the matrix and Fe solvent from the matrix into the precipitates by ballistic dissolution.

Previous studies suggest that CrRP form in a radiation enhanced precipitation mechanism [10 , 12 , 13 , 24 , 26]. This mechanism explains the accelerated cluster formation under electron irradiation, dur- ing which there is no appreciable ballistic dissolution of Cr clus- ter nuclei and the cluster Cr content could reach > 90 at.% [24] . However, after neutron irradiation at the same temperature, the cluster solute concentration was reduced to about 85 at.% and the cluster sizes are smaller [10] . A further discrepancy in the Cr so- lute content and precipitate size occurs for the high dose rate heavy ion irradiation results, in which cluster absence or clusters with much lower Cr content were observed. Considering the re- ported results and our observations, there is strong evidence that the steady state condition for CrRP precipitation under ion or neu- tron irradiations at 300–450 °C is controlled by the irradiation con- ditions, as originally suggested by Nelson et al. [32] . Based on the comparison of the precipitate evolution in annealed vs. aged Fe- 18Cr at 300–350 °C (Figs. 7-9), quasi-equilibrium CrRP distributions are achieved already at doses below 1 dpa. Due to the presence of ballistic dissolution in these energetic displacement cascade con- ditions, radiation enhanced precipitation, which considers only the accelerated diffusion due to irradiation, is not solely appropriate to explain the CrRP precipitation behavior. Since the precipitate size, number density, and solute concentration all deviated from their thermal equilibrium values, the radiation modified precipi- tation

processes seem to be more suitable for describing the observed evolution.

It must be pointed out that although the formation of CrRP with sub-equilibrium Cr content is similar to the traditional radi- ation modified precipitation phenomenon, the underlying mecha- nisms are different. The radiation modified precipitation phenom- ena were first proposed in the 1980s and involved the contribution from radiation induced solute segregation (RIS) [90] . Based on our current study and related prior studies, RIS processes do not ap- pear to be playing a dominant role in CrRP evolution during irradi- ation [91 , 92]. According to refs. [10–13 , 26–28,93] and our results, CrRP were observed to be distributed homogeneously in the matrix without clear association with visible point defect sinks. Although chromium enrichment has been observed at dislocation loops in irradiated FeCr alloys [23 , 58], the Cr content at the loops after heavy ion irradiation was ~22–35%, which is much lower than the Cr content of CrRP, and it was tentatively explained to be related to stabilization of Cr clusters by impurities, so its effect on CrRP precipitation remains unclear for now [58] . Although the chemi- cal compositions of precipitates during irradiation can generally be changed by either RIS or ballistic mixing/dissolution processes, the lack of direct relation of CrRP with defect sinks, and the consistent trends regarding Cr concentrations in precipitates and matrix with respect to irradiation temperatures and dose rates in the FeCr alloy systems indicates that the change of Cr content, quasi-equilibrium precipitate size and number density primarily results from competition between radiation enhanced diffusion and ballistic dissolution, instead of the preferential coupling between point defects and Cr atoms.

The radiation modified precipitation behavior of CrRP generally occurs at all irradiation conditions. The extent to which the steady state precipitate parameters are modified from their thermal equilibrium state is determined by the irradiation conditions including temperature, dose rate and the type of injected particles. During irradiations performed with protons or electrons, only minor deviations from the thermal equilibrium steady state are anticipated due to the absence of displacement cascades. In other words, the precipitate evolution will be closer to a pure radiation enhanced precipitation behavior, in which accelerated kinetics is most important. During neutron or heavy ion irradiations that in- volves displacement cascades, we observed that higher dose rates tend to slow down the Ostwald ripening rate and lead to a final steady state with finer and less solute-concentrated precipitates. Hence, the characteristics of precipitates could all be potentially modified depending on the balance between the rates of disso- lution and back diffusion. The effect of increasing dose rate be- comes more pronounced at low temperatures, and could result in the complete dissolution of precipitates. Although ion irradiation is a powerful tool to study radiation related effects and to test the ir- radiation tolerance of materials, the dose rates normally used during ion irradiations are 3–4 orders of magnitude higher than what is relevant for fission or fusion reactor conditions. Since the irradi- ation dose rate has a significant effect on the stability of precipi- tates, great care must be taken to extrapolate the results obtained from ion irradiation studies to neutron irradiation conditions. The possible stabilization of detrimental precipitates and coarsening of beneficial ones at lower dose rates must be considered for designing precipitate-containing materials for reactor applications
[94] .

5. Conclusions

In this study, Fe-18Cr specimens were irradiated with 8 MeV Fe ions at a variety of conditions including dose rates

of 10^{-5}–10^{-3} dpa/s, temperatures of 300–450 °C, and final midrange doses of 0.37 and 3.7 dpa. CrRP formed after most irradiations performed in this study and they were characterized with APT. Analysis of APT datasets was completed with IVAS and a solute concentration- based cluster searching algorithm developed by the authors, which was found to provide improved self-consistent results compared to the conventional maximum separation method. The main conclu- sions are summarized here:

(1) The critical ion irradiation condition for CrRP to dissolve in Fe- 18Cr is 300 °C and 10^{-3} dpa/s, which is consistent with ear- lier experimental results. This behavior was correctly explained by a modified NHM model concerning the competition be- tween radiation enhanced diffusion (precipitate re-nucleation, growth and coarsening) and ballistic dissolution (precipitate shrinkage). An error in the original NHM model was corrected and several important modifications for this model were in- troduced: using a more accurate estimation of the number of recoils per dpa, which is more than two orders of magni- tude larger than assumed in the original NHM model due to an incorrect displacement cross-section for medium-mass ions and neglect of the RPA atomic mixing concept in the original NHM model, consideration of thermal equilibrium solubility effects, and the available matrix volume fractions, which result in a much better correlation to the experimental observations. However, due to the several assumptions used to simplify this model, adjustment of the ballistic dissolution rate might be needed if effects such as impurity atoms, sink strength of carbides and dislocations, and CrRP number density change are considered.

(2) At irradiation conditions with higher temperatures or lower dose rates compared to the critical values, the precipitates were observed to nucleate and grow. The precipitate radii gener- ally increase with increasing temperature and decrease with in- creasing dose rate. The number density of CrRP was highest at 350 °C and decreases with increasing dose rate at all tempera- tures. These trends generally agree with the nucleation, growth and coarsening of precipitates (modified by ballistic dissolution and radiation enhanced diffusion effects). The Cr concentration in the CrRP and matrix shows larger deviations compared to their thermal equilibrium values for irradiations at lower tem- peratures or higher dose rates, which indicates an increasing importance of ion mixing.

(3) Increasing the irradiation dose from 0.37 to 3.7 dpa led to only slight growth of CrRP at 350 °C, while significant coarsening was observed at 450 °C, which is attributable to the differ- ence in diffusion rates at these two temperatures. The existence of well-developed CrRP before irradiation has a negligible ef- fect on the precipitate size and number density after irradi- ation at 300–350 °C, which agrees with the behavior quanti- tatively predicted by the modified NHM model. This indicates that equilibrium cluster size is typically controlled by irradi- ation conditions irrespective of the initial starting microstruc- tural state (annealed vs. aged), and the steady state can be achieved relatively quickly within 0.3–0.4 dpa under the in- vestigated 300–350 °C, 10^{-3} dpa/s irradiation conditions. How- ever, a convergent precipitate distribution was not achieved between the annealed and aged specimen after irradiation at 450 °C to 0.37 dpa, which deviated from the modified NHM model prediction, and was attributed to the higher recovery rate at this higher temperature. Both sets of observations sug- gest that ballistic dissolution processes produce quasiequilib- rium within 0.3–0.4 dpa at low to intermediate temperatures, whereas normal thermal coarsening processes dominate at high temperatures.

(4) Combining our results with data available in the literature, it is found that the cluster size is more sensitive to irradiation temperature than dose rate. Larger solute clusters were invari- ably observed at higher temperatures. However, the solute con- centration in clusters is more strongly influenced by dose rate than temperature. Although we observed the precipitate num- ber density to decrease with increasing dose rate, no clear con- clusion can be drawn when multiple studies are compared to- gether, which might be attributed to the large difference in ion energies,

post-irradiation characterization methods and APT data analysis methods.

(5) All the CrRP observed after ion irradiation have Cr concentra- tions well below the equilibrium value, and the correspond- ing matrix Cr contents are well above the solvus concentra- tion limit. This can be attributed to kinetic aspects of either non-classical nucleation mechanism or the continuous ion mix- ing between the precipitate and matrix atoms by energetic dis- placement cascades. Radiation modified precipitation processes appear to correctly account for this behavior. The competition between radiation enhanced diffusion and ballistic dissolution provides a second path to produce a steady state different than thermal equilibrium compared to the traditional path through RIS. Both the size and solute concentration in precipitates were modified by the presence of displacement cascades. The effect of dose rate on precipitate stability is pronounced at typical ion irradiation conditions and must be considered when extrapolating high dose rate results for possible applications under lower dose rate fission or fusion reactor environments.

Declaration of Competing Interest

The authors declare that they have no known competing finan- cial interests or personal relationships that could have appeared to influence the work reported in this paper.

Acknowledgements

The authors would like to thank Dr. Philip Edmondson and Mr. James P. Burns from ORNL for helping with APT data acquisition and analysis. We thank Ovidiu Toader and the Michigan Ion Beam Laboratory team for their assistance in performing the ion irradia- tions.

Funding: This research was sponsored by the Office of Fusion Energy Sciences, U.S. Department of Energy under grant # DE- SC0 0 0 6 6 61 with the University of Tennessee (YZ, SJZ) and con- tract DE-AC05–00OR22725 with UT-Battelle, LLC (AB). The authors would like to acknowledge funding from the State of Tennessee and Tennessee Higher Education Commission (THEC) through their support of the Center for Materials Processing. The fabrication of the Fe-Cr binary alloys has been carried out within the framework of the EUROfusion Consortium and has received funding from the Euratom research and training program 2019–2020 under Grant Agreement No. 633053. APT was conducted at ORNL's Center for Nanophase Materials Sciences (CNMS), which is a U.S. DOE Office of Science User Facility.

Supplementary materials

Supplementary material associated with this article can be found, in the online version, at doi: 10.1016/j.actamat.2022.117888 .

References

[1] R.L. Klueh , D.R. Harries , High-chromium Ferritic and Martensitic Steels For Nu- clear Applications, 2001 AsTM West Conshohocken, PA .
[2] Z. Jiao , V. Shankar , G.S. Was , Phase stability in proton and heavy ion irradiated ferritic–martensitic alloys, J. Nucl. Mater. 419 (1–3) (2011) 52–62 .
[3] D. Chen , A. Kimura , W. Han , Correlation of Fe/Cr phase decomposition process and age-hardening in Fe–15Cr ferritic alloys, J. Nucl. Mater. 455 (1–3) (2014) 436–439 .
[4] P. Grobner , The 885 F (475 C) embrittlement of ferritic stainless steels, Metall. Trans. 4 (1) (1973) 251–260 .
[5] R. Fisher , E. Dulis , K. Carroll , Identification of the precipitate accompanying 885-Degrees-F embrittlement in chromium steels, Trans. Am. Inst. Min. Metal- lurg. Eng. 197 (5) (1953) 690–695 .
[6] M. Miller , R. Stoller , K. Russell , Effect of neutron-irradiation on the spin- odal decomposition of Fe-32% Cr model alloy, J. Nucl. Mater. 230 (3) (1996) 219–225 .
[7] S. Novy , P. Pareige , C. Pareige , Atomic scale analysis and phase separation understanding in a thermally aged Fe–20at.%Cr alloy, J. Nucl. Mater. 384 (2) (2009) 96–102 .
[8] O. Tissot , C. Pareige , M.H. Mathon , M. Roussel , E. Meslin , B. Décamps , J. Henry , Comparison between SANS and APT measurements in a thermally aged Fe-19 at.%Cr alloy, Mater. Charact. 151 (2019) 332–341 .
[9] C. Pareige , S. Novy , S. Saillet , P. Pareige , Study of phase transformation and me-chanical properties evolution of duplex stainless steels after long term thermal ageing (>20years), J. Nucl. Mater. 411 (1–3) (2011) 90–96 .
[10] M. Bachhav , G. Robert Odette , E.A. Marquis , α' precipitation in neutron-irradi- ated Fe–Cr alloys, Scr. Mater. 74 (2014) 48–51 .
[11] E.R. Reese , M. Bachhav , P. Wells , T. Yamamoto , G.. Odette , E.A. Marquis , On α' precipitate composition in thermally annealed and neutron-irradiated Fe- 9-18Cr alloys, J. Nucl. Mater. 500 (2018) 192–198 .
[12] V. Kuksenko , C. Pareige , P. Pareige , Cr precipitation in neutron irradiated in- dustrial purity Fe–Cr model alloys, J. Nucl. Mater. 432 (1–3) (2013) 160–165 .
[13] F. Bergner , A. Ulbricht , C. Heintze , Estimation of the solubility limit of Cr in Fe at 300 °C from small-angle neutron scattering in neutron-irradiated Fe–Cr alloys, Scr. Mater. 61 (11) (2009) 1060–1063 .

[14] W.-.Y. Chen , Y. Miao , Y. Wu , C.A. Tomchik , K. Mo , J. Gan , M.A. Okuniewski , S.A. Maloy , J.F. Stubbins , Atom probe study of irradiation-enhanced α' pre- cipitation in neutron-irradiated Fe–Cr model alloys, J. Nucl. Mater. 462 (2015) 242–249 .

[15] M.H. Mathon , Y. de Carlan , G. Geoffroy , X. Averty , A. Alamo , C.H. de Novion , A SANS investigation of the irradiation-enhanced α- α' phases separation in 7–12 Cr martensitic steels, J. Nucl. Mater. 312 (2–3) (2003) 236–248 .

[16] P. Dubuisson , D. Gilbon , J.L. Seran , Microstructural evolution of ferritic-martensitic steels irradiated in the fast breeder reactor Phenix, J. Nucl. Mater. 205 (1993) 178–189 .

[17] D.S. Gelles , Microstructural examination of neutron-irradiated simple ferritic alloys, J. Nucl. Mater. 108 (1982) 515–526 .

[18] D.S. Gelles , Microstructural examination of several commercial alloys neutron irradiated to 100 dpa, J. Nucl. Mater. 148 (2) (1987) 136–144 .

[19] D.S. Gelles , Microstructural development in reduced activation ferritic alloys irradiated to 200 dpa at 420 C, J. Nucl. Mater. 212 (1994) 714–719 .

[20] Y. Katoh , A. Kohyama , D.S. Gelles , Swelling and dislocation evolution in sim- ple ferritic alloys irradiated to high fluence in FFTF/MOTA, J. Nucl. Mater. 225 (1995) 154–162 .

[21] D.S. Gelles , Void swelling in binary FeCr alloys at 200 dpa, J. Nucl. Mater. 225 (1995) 163–174 .

[22] D.S. Gelles , Microstructural examination of commercial ferritic alloys at 200 dpa, J. Nucl. Mater. 233 (1996) 293–298 .

[23] E. Wakai , A. Hishinuma , Y. Kato , H. Yano , S. Takaki , K. Abiko , Radiation-Induced α' Phase Formation on Dislocation Loops in Fe-Cr Alloys During Electron Irra- diation, Le J. Phys. IV 05(C7) (1995) C7-277-C7-286 .

[24] O. Tissot , C. Pareige , E. Meslin , B. Decamps , J. Henry , Kinetics of α' precipitation in an electron-irradiated Fe15Cr alloy, Scr. Mater. 122 (2016) 31–35 .

[25] E. Marquis, B. Wirth, G. Was, Characterization and Modeling of Grain Boundary Chemistry Evolution in Ferritic Steels Under Irradiation, United States, (2016) doi: 10.2172/1248953 .

[26] O. Tissot , C. Pareige , E. Meslin , B. Décamps , J. Henry , Influence of injected in- terstitials on α' precipitation in Fe–Cr alloys under self-ion irradiation, Mater. Res. Lett. 5 (2) (2016) 117–123 .

[27] R.W. Harrison , A.W. Carruthers , J.A. Hinks , M.G. Burke , S.E. Donnelly , Cascade size and dose rate effects on α' precipitation in ion-irradiated Fe14Cr alloy, Scr. Mater. 172 (2019) 33–37 .

[28] E.R. Reese , N. Almirall , T. Yamamoto , S. Tumey , G.R. Odette , E.A. Marquis , Dose rate dependence of Cr precipitation in an ion-irradiated Fe 18Cr alloy, Scr. Mater. 146 (2018) 213–217 .

[29] F. Soisson , E. Meslin , O. Tissot , Atomistic modeling of α' precipitation in Fe-Cr alloys under charged particles and neutron irradiations: effects of ballistic mix- ing and sink densities, J. Nucl. Mater. 508 (2018) 583–594 .

[30] C. Pareige , V. Kuksenko , P. Pareige , Behaviour of P, Si, Ni impurities and Cr in self ion irradiated Fe–Cr alloys – Comparison to neutron irradiation, J. Nucl. Mater. 456 (2015) 471–476 .

[31] G. Bonny , D. Terentyev , L. Malerba , On the α- α' miscibility gap of Fe–Cr alloys, Scr. Mater. 59 (11) (2008) 1193–1196 .

[32] R. Nelson , J. Hudson , D. Mazey , The stability of precipitates in an irradiation environment, J. Nucl. Mater. 44 (3) (1972) 318–330 .

[33] S. Zinkle , G. Kulcinski , L. Mansur , Radiation-enhanced recrystallization in cop- per alloys, J. Nucl. Mater. 141 (1986) 188–192 .

[34] R.S. Averback , Fundamental aspects of ion beam mixing, Nucl. Instrum. Meth- ods Phys. Res. Sect. B 15 (1–6) (1986) 675–687 .

[35] R. Averback , Atomic displacement processes in irradiated metals, J. Nucl. Mater. 216 (1994) 49–62 .

[36] H.J. Frost , K.C. Russell , Particle stability with recoil resolution, Acta Metall. 30 (5) (1982) 953–960 .

[37] G. Martin , Phase stability under irradiation: ballistic effects, Phys. Rev. B 30 (3) (1984) 1424 .

[38] P. Bellon , Precipitate and microstructural stability ináalloys subjected to sus- tained irradiation, in: Materials Science with Ion Beams, Springer, 2009, pp. 29–52 .

[39] J.-.O. Andersson , B. Sundman , Thermodynamic properties of the Cr-Fe system, Calphad 11 (1) (1987) 83–92 .

[40] O. Senninger , E. Martínez , F. Soisson , M. Nastar , Y. Bréchet , Atomistic simula- tions of the decomposition kinetics in Fe–Cr alloys: influence of magnetism, Acta Mater. 73 (2014) 97–106 .

[41] C. Heintze , F. Bergner , A. Ulbricht , H. Eckerlebe , The microstructure of neu- tron-irradiated Fe–Cr alloys: a small-angle neutron scattering study, J. Nucl. Mater. 409 (2) (2011) 106–111 .

[42] P.D. Edmondson , S.A. Briggs , Y. Yamamoto , R.H. Howard , K. Sridharan , K.A. Ter- rani , K.G. Field , Irradiation-enhanced α' precipitation in model FeCrAl alloys, Scr. Mater. 116 (2016) 112–116 .

[43] S. Agarwal , Y. Lin , C. Li , R. Stoller , S. Zinkle , On the use of SRIM for calculating vacancy production: quick calculation and full-cascade options, Nucl. Instrum. Methods Phys. Res. Sect. B 503 (2021) 11–29 .

[44] S.J. Zinkle , L.L. Snead , Opportunities and limitations for ion beams in radiation effects studies: bridging critical gaps between charged particle and neutron irradiations, Scr. Mater. 143 (2018) 154–160 .

[45] A.M. Monterrosa , D. Woodley , Z. Jiao , G.S. Was , The influence of carbon on cavity evolution in ion-irradiated ferritic-martensitic steels, J. Nucl. Mater. 509 (2018) 722–735 .

[46] M. Thuvander , H.-.O. Andren , K. Stiller , Q.-.H. Hu , A statistical method to de- tect ordering and phase separation by APFIM, Ultramicroscopy 73 (1998) 7 .

[47] O.C. Hellman , J.A. Vandenbroucke , J. Rüsing , D. Isheim , D.N. Seidman , Analysis of three-dimensional atom-probe data by the proximity histogram, Microsc. Microanal. 6 (5) (20 0 0) 437–4 4 4 .

[48] V. Kuksenko , C. Pareige , C. Genevois , F. Cuvilly , M. Roussel , P. Pareige , Effect of neutron-irradiation on the microstructure of a Fe–12at.%Cr alloy, J. Nucl. Mater. 415 (1) (2011) 61–66 .

[49] J.M. Hyde , G. DaCosta, C. Hatzoglou , H. Weekes , B. Radiguet , P.D. Styman, F. Vurpillot , C. Pareige , A. Etienne , G. Bonny , N. Castin , L. Malerba , P. Pareige , Analysis of radiation damage in light water reactors: comparison of cluster analysis methods for the analysis of atom probe data, Microsc. Microanal. 23 (2) (2017) 366–375 .

[50] D. Haley, 3Depict - Visualisation & Analysis for Atom Probe, 2010 http://threedepict.sourceforge.net .

[51] P.D. Styman , J.M. Hyde , K. Wilford , G.D. Smith , Quantitative methods for the APT analysis of thermally aged RPV steels, Ultramicroscopy 132 (2013) 258–264 .

[52] D. Vaumousse , A. Cerezo , P. Warren , A procedure for quantification of precipi- tate microstructures from three-dimensional atom probe data, Ultramicroscopy 95 (2003) 215–221 .

[53] L. Malerba , A. Caro , J. Wallenius , Multiscale modelling of radiation damage and phase transformations: the challenge of FeCr alloys, J. Nucl. Mater. 382 (2–3) (2008) 112–125 .

[54] A. Baldan , Review progress in Ostwald ripening theories and their applications to nickel-base superalloys Part I: ostwald ripening theories, J. Mater. Sci. 37 (11) (2002) 2171–2202 .

[55] M.L. Jenkins , Z. Yao , M. Hernández-Mayoral , M.A. Kirk , Dynamic observations of heavy-ion damage in Fe and Fe–Cr alloys, J. Nucl. Mater. 389 (2) (2009) 197–202 .

[56] S. Xu , Z. Yao , M.L. Jenkins , TEM characterisation of heavy-ion irradiation dam- age in FeCr alloys, J. Nucl. Mater. 386-388 (2009) 161–164 .

[57] A. Bhattacharya , E. Meslin , J. Henry , A. Barbu , S. Poissonnet , B. Décamps , Effect of chromium on void swelling in ion irradiated high purity Fe–Cr alloys, Acta Mater 108 (2016) 241–251 .

[58] A. Bhattacharya , E. Meslin , J. Henry , C. Pareige , B. Décamps , C. Genevois , D. Brimbal , A. Barbu , Chromium enrichment on the habit plane of dislocation loops in ion-irradiated high-purity Fe–Cr alloys, Acta Mater 78 (2014) 394–403 .

[59] F. Soisson , T. Jourdan , Radiation-accelerated precipitation in Fe–Cr alloys, Acta Mater 103 (2016) 870–881 .

[60] J.-.H. Ke , E.R. Reese , E.A. Marquis , G.R. Odette , D. Morgan , Flux effects in pre- cipitation under irradiation – Simulation of Fe-Cr alloys, Acta Mater 164 (2019) 586–601 .

[61] G.S. Was, Fundamentals of Radiation Materials science: Metals and Alloys, springer 2016.

[62] L. Mansur , Theory and experimental background on dimensional changes in irradiated alloys, J. Nucl. Mater. 216 (1994) 97–123 .

[63] K. Nakashima , R.E. Stoller , H. Xu , Recombination radius of a Frenkel pair and capture radius of a self-interstitial atom by vacancy clusters in bcc Fe, J. Phys. Condens. Matter. 27 (33) (2015) 335401 .

[64] C.C. Fu , F. Willaime , First principles calculations in iron: structure and mobility of defect clusters and defect complexes for kinetic modelling, C. R. Phys. 9 (3–4) (2008) 335–342 .

[65] S. Zinkle , B. Singh , Analysis of displacement damage and defect production un- der cascade damage conditions, J. Nucl. Mater. 199 (3) (1993) 173–191 .

[66] S.J. Zinkle , R.E. Stoller , On the importance of thermally stimulated correlated defect recombination in radiation effects studies, J. Nucl. Mater. (2022) sub- mitted .

[67] K. Nordlund , S.J. Zinkle , A.E. Sand , F. Granberg , R.S. Averback , R.E. Stoller , T. Suzudo , L. Malerba , F. Banhart , W.J. Weber , F. Willaime , S.L. Dudarev , D. Simeone , Primary radiation damage: a review of current understanding and models, J. Nucl. Mater. 512 (2018) 450–479 .

[68] F.S. Ham , Theory of diffusion-limited precipitation, J. Phys. Chem. Solids 6 (4) (1958) 335–351 .

[69] G. Kulcinski , J. Brimhall , H. Kissinger , Production of Voids in Pure Metals by High-Energy Heavy-Ion Bombardment, Pacific Northwest Lab., Battelle-North- west, Richland, Wash, 1971 .

[70] J.F. Ziegler , M.D. Ziegler , J.P. Biersack , SRIM–The stopping and range of ions in matter (2010), Nucl. Instrum. Methods Phys. Res. Sect. B 268 (11–12) (2010) 1818–1823 .

[71] K. Nordlund , S.J. Zinkle , A.E. Sand , F. Granberg , R.S. Averback , R. Stoller , T. Suzudo , L. Malerba , F. Banhart , W.J. Weber , Improving atomic displacement and replacement calculations with physically realistic damage models, Nat. Commun. 9 (1) (2018) 1–8 .

[72] S. Agarwal, S.J. Zinkle, Experimental studies on primary damage formation, in: R. Konings, R. Stoller (Eds.), Comprehensive Nuclear Materials, 2nd Ed., Else- vier, Oxford, 2020, pp. 74–90.

[73] A. Marwick , Solute segregation and precipitate stability in irradiated alloys, Nucl. Instrum. Methods 182 (1981) 827–843 .

[74] R.A. Enrique , K. Nordlund , R.S. Averback , P. Bellon , Simulations of dynamical stabilization of Ag–Cu nanocomposites by ion-beam processing, J. Appl. Phys. 93 (5) (2003) 2917–2923 .

[75] R.S. Averback , T. Diaz De , La Rubia , Displacement damage in irradiated metals and semiconductors, Solid State Phys. 51 (1997) 281–402 .

[76] C. Domain , C. Becquart , J. Foct , Ab initio study of foreign interstitial atom (C, N) interactions with intrinsic point defects in α-Fe, Phys. Rev. B 69 (14) (2004) 144112 .

[77] C.J. Först , J. Slycke , K.J. Van Vliet , S. Yip , Point defect concentrations in metastable Fe-C alloys, Phys. Rev. Lett. 96 (17) (2006) 175501 .

[78] M. Konstantinovi c´ , L. Malerba , Dissolution of carbon-vacancy complexes in Fe-C alloys, Phys. Rev. Mater. 1 (5) (2017) 053602 .

[79] B. Minov , M. Lambrecht , D. Terentyev , C. Domain , M. Konstantinovi c´ , Structure of nanoscale copper precipitates in neutron-irradiated Fe-Cu-C alloys, Phys. Rev. B 85 (2) (2012) 024202 .

[80] E. Meslin , A. Barbu , L. Boulanger , B. Radiguet , P. Pareige , K. Arakawa , C. Fu, Cluster-dynamics modelling of defects in α-iron under cascade damage condi- tions, J. Nucl. Mater. 382 (2–3) (2008) 190–196 .
[81] P. Zhu , Y. Zhao , S. Agarwal , J. Henry , S.J. Zinkle , Toward accurate evaluation of bulk hardness from nanoindentation testing at low indent depths, Mater. Design 213 (2022) 110317 .
[82] D. Potter , D. Ryding , Precipitate coarsening, redistribution and renucleaton dur- ing irradiation of Ni-6.35wt.% Al, J. Nucl. Mater. 71 (1) (1977) 14–24 .
[83] M.L. Lescoat , J. Ribis , Y. Chen , E.A. Marquis , E. Bordas , P. Trocellier , Y. Ser- ruys , A. Gentils , O. Kaïtasov , Y. de Carlan , A. Legris , Radiation-induced Ostwald ripening in oxide dispersion strengthened ferritic steels irradiated at high ion dose, Acta Mater 78 (2014) 328–340 .
[84] F. Vurpillot , A. Bostel , D. Blavette , Trajectory overlaps and local magnification in three-dimensional atom probe, Appl. Phys. Lett. 76 (21) (20 0 0) 3127–3129 .
[85] V. Kuksenko , Model Oriented Irradiation Experiments in Fe-Cr model Alloys, Université de Rouen, 2011 .
[86] C. Hatzoglou , B. Radiguet , G. Da Costa , P. Pareige , M. Roussel , M. Hernan- dez-Mayoral , C. Pareige , Quantification of APT physical limitations on chemi- cal composition of precipitates in Fe–Cr alloys, J. Nucl. Mater. 522 (2019) 64– 73 .
[87] P. L'vov , V. Svetukhin , A. Obukhov , Thermodynamics of phase equilibrium of binary alloys containing nanprecipitates, Phys. Solid State 53 (2) (2011) 421–427 .
[88] J.D. Robson , Modelling the overlap of nucleation, growth and coarsening dur- ing precipitation, Acta Mater 52 (15) (2004) 4669–4676 .
[89] V. Svetukhin , P. L'vov , E. Gaganidze , M. Tikhonchev , C. Dethloff, Kinetics and thermodynamics of Cr nanocluster formation in Fe–Cr system, J. Nucl. Mater. 415 (2) (2011) 205–209 .
[90] A. Rowcliffe , E.H. Lee , High temperature radiation damage phenomena in com- plex alloys, J. Nucl. Mater. 108 (1982) 306–318 .
[91] M. Nastar , F. Soisson , Radiation-induced segregation, in: R. Konings (Ed.), Comprehensive Nuclear Materials, Elsevier, Amsterdam, 2012, pp. 471–496 .
[92] J. Ribis , Phase stability in irradiated alloys, in: R. Konings, R. Stoller (Eds.), Comprehensive Nuclear Materials, 2nd Ed., Elsevier, Oxford, 2020, pp. 265–309 .
[93] F. Bergner , C. Pareige , V. Kuksenko , L. Malerba , P. Pareige , A. Ulbricht , A. Wagner , Critical assessment of Cr-rich precipitates in neutron-irradiated Fe–12at%Cr: comparison of SANS and APT, J. Nucl. Mater. 442 (1–3) (2013) 463–469 .
[94] G. Odette , M. Alinger , B. Wirth , Recent developments in irradiation-resistant steels, Annu. Rev. Mater. Res. 38 (2008) 471–503 .